

Chemical Properties of Star Forming Dwarf Galaxies

Ovidiu Vaduvescu¹

*Instituto de Astronomía, Universidad Católica del Norte
Avenida Angamos 0610, Antofagasta, Chile
Former address: ACRU & SAAO, University of KwaZulu-Natal,
School of Mathematical Sciences, Durban 4041, South Africa*

Marshall L. McCall²

*York University, Department of Physics and Astronomy
4700 Keele Street, M3J 1P3, Toronto, ON, Canada*

Michael G. Richer³

*Observatorio Astrónomico Nacional, Instituto de Astronomía
Universidad Nacional Autónoma de México
PO Box 439027, San Diego, CA 92143-9027, USA*

ABSTRACT

Recent studies of the near-infrared (NIR) properties of dwarf irregular galaxies (dIs) and blue compact dwarfs (BCDs) have provided improved estimates for the NIR luminosity of old stellar populations in these galaxies. These can be used to derive gas fractions, and thereby to evaluate how BCDs have evolved with respect to dIs. Oxygen abundances have been derived for four BCDs in the Virgo Cluster from a run at Gemini-North in 2003. Combining these new abundances with published values, we study the correlations among the metallicity, K_s luminosity, gas mass, baryonic mass, and gas fraction. Within errors, the two types of dwarfs appear to share a common relation between the oxygen abundance and the luminosity in K_s . The correlation between metallicity and the gas fraction

¹email: ovidiuv@yahoo.com

²email: mccall@yorku.ca

³email: richer@astrosen.unam.mx

is the same for BCDs as for dIs, indicating that BCD evolution has been similar to dIs. Since dIs appear to have evolved as isolated systems, the BCD bursts are unlikely to be a consequence of gas infall or merging.

Subject headings: galaxies: dwarf irregulars, blue compact dwarfs; galaxies: evolution; near-infrared; luminosity; mass; metallicity; gas fractions.

1. Introduction

1.1. A Universe of Dwarfs

Dwarf galaxies are by far the most numerous galaxies in the Universe. About 80–90 per cent of the members of the Local Group are classified as dwarfs (Mateo 1998; Grebel 2000), while about 85 per cent of the known galaxies in the Local Volume ($D \lesssim 10$ Mpc) are also dwarfs (Karachentsev et al. 2004). The space density of dwarfs in the Universe has been suggested to be about 40 times that of bright galaxies (Stavely-Smith, Davies, & Kinman 1992).

Dwarf galaxies are defined arbitrarily as galaxies having an absolute magnitude fainter than $M_B \sim -16$ mag (Tammann 1994) or $M_V \sim -18$ mag (Grebel 2000, 2001). Based on their optical appearance, dwarf galaxies can be classified into five groups: dwarf irregulars (dIs), blue compact dwarfs (BCDs), dwarf ellipticals (dEs), dwarf spheroidals (dSphs), and dwarf spirals (dS’s). The distinction between dEs and dSphs is not clear (e.g., Bingelli 1994), while dS’s can be regarded as the very small end of spirals (Matthews and Gallagher 1997; Grebel 2001). Excluding dS’s, dIs and BCDs are the only systems harboring active or recent star formation activity. According to hierarchical clustering models of galaxy formation, larger galactic structures build up and grow through the accretion of dwarf galaxies (White and Frenk 1991; Kauffmann, White, & Guiderdoni 1993). Nevertheless, some recent evidence (e.g., Venn et al. 2004; Helmi et al. 2006) suggests that the halo of the Milky Way could not have been constructed from dSphs as we presently know them. In this picture, dIs and BCDs may be similar to the building blocks for more massive galaxies. As such, they are important probes for studying matter in its near-primordial state, thus being relevant to understanding galaxy formation and evolution.

Despite the advances in the last decades, the relation between dIs and BCDs remains unclear. Some authors suggest that BCDs and dIs are the same type of galaxy, with BCDs being dIs undergoing bursts of star formation (e.g. Thuan 1985). Others argue that dIs are a fundamentally distinct type from BCDs, with no simple evolutionary links between

them (e.g., James 1994). Richer and McCall (1995) argued on chemical grounds that BCDs may be more akin to dSphs than dIs. Papaderos et al. (1996a) review previous arguments concerning the evolutionary relationships between BCDs, dIs and dEs without reaching firm conclusions.

1.2. Determining Chemical Abundances for Dwarfs

The *metallicity*, Z , is defined as the fraction of elements other than hydrogen and helium by mass (e.g., Pagel 1997). Metallicity is a key parameter intimately linked to the formation and evolution of galaxies. It gives an indication of age in the sense that it reveals how far the conversion of gas into stars has proceeded. In practice, the metallicity in star-forming galaxies is quantified via the *oxygen abundance*, defined as the fraction of oxygen by number, $12 + \log(n(\text{O})/n(\text{H}))$. After hydrogen and helium, the most abundant element in the Universe is oxygen. It is convenient to measure the oxygen abundance because it exhibits emission lines in HII region spectra which are very bright and easy to measure.

Physical and chemical properties of nebulae can be derived by measuring ratios of intensities of collisionally-excited emission lines (e.g., Osterbrock 1989). Recombination lines of metals are normally too faint to detect in extragalactic nebulae, though in some of the very brightest objects recombination lines have been detected (e.g., Peimbert et al. 2006). The radiation emitted by a nebula depends upon the abundances of the chemical elements and the physical state of the gas, especially its average temperature and density.

A natural reference for elemental abundances is the Sun, which has an oxygen abundance, $12 + \log(\text{O}/\text{H})_{\odot} = 8.69$ (e.g., Allende Prieto, Lambert, & Asplund 2001). We define $Z_{\odot} = (\text{O}/\text{H})_{\odot}$. It is customary to define “metal poor” as a system with an abundance lower than this value, and “metal-rich” as a system with an abundance exceeding this value. dIs and BCDs are the most metal-poor galaxies, having metallicities as low as $\sim 1/50 Z_{\odot}$. In high-redshift clouds of gas, which may be building blocks of today’s galaxies, the metallicity can reach values as low as $0.001 Z_{\odot}$ (Kunth and Ostlin 2000). Stars in our Galaxy reach metallicities as low as $0.00001 Z_{\odot}$ (Sparke and Gallagher 2000).

There are two commonly-used methods to determine oxygen abundances in HII regions. The *direct method* (T_e) is founded upon a direct measurement of temperature. It is applicable whenever the temperature diagnostic $[\text{O III}]\lambda 4363$ is detectable and in which the doubly ionized O^{+2} ion represents the dominant form of oxygen (Osterbrock 1989). The most accurate oxygen abundances are derived using the direct method, but for most galaxies $[\text{O III}]\lambda 4363$ is faint and difficult to detect. When $[\text{O III}]\lambda 4363$ is not detected, the *bright-line method*

(R_{23}), originally proposed by Pagel et al. (1979), is commonly used. The oxygen abundance is parametrized as a function of the ratio $R_{23} = (I[\text{OII}]\lambda 3727 + I[\text{OIII}]\lambda\lambda 4959, 5007)/I(\text{H}\beta)$. Unfortunately, the R_{23} indicator is not a monotonic function of oxygen abundance; for a given value of R_{23} , two values of the oxygen abundance are possible. However, McGaugh (1991) suggested that $\log([\text{NII}]\lambda 6583/[\text{OII}]\lambda 3727)$ can be used as a discriminator between the lower and upper branches. To estimate oxygen abundances, we adopt the calibration of R_{23} developed by McGaugh (1994), which employs $O_{32} = I([\text{OIII}]\lambda 4959, 5007)/I([\text{OII}]\lambda 3727)$ to discriminate between the two branches.

1.3. Dwarfs and the Closed Box Model

One of the simplest frameworks for galaxy evolution is the *closed box model* (Searle and Sargent 1972; Pagel 1997). According to this model, a galaxy consists initially of gas with no stars and no metals. The stellar initial mass function (IMF) is assumed to be constant in time. Stars that end their life as supernovae are assumed to enrich the interstellar gas with metals immediately, thereby eliminating time as a variable. Throughout the entire time, the galaxy evolves as a closed system, with no mass inflow or outflow. For such a system, the metallicity at any given time is solely determined by the fraction of baryons which remains in gaseous form, which is referred to as the *gas fraction*.

Many researchers, starting with Lequeux et al. (1979), have examined how the metallicity of a galaxy depends upon its mass or luminosity, finding that more massive galaxies are more abundant in metals. Skillman, Kennicutt, & Hodge (1989) confirmed a strong correlation between absolute magnitude and metallicity for local dIs, in the sense that the least luminous dIs are the most metal-poor systems. Richer and McCall (1995) derived a more robust $L_B - Z$ relationship, based on a sample of 25 nearby irregular galaxies having well-determined and self-consistent distances along with abundances calculated from measured [O III] temperatures. An enlarged sample was considered by Miller and Hodge (1996), with the same conclusions. The same correlation was found by van Zee, Haynes, & Salzer (1997) in another sample of 15 gas-rich, low surface brightness dwarfs.

Information about the chemical evolution of dwarf galaxies is buried within the $L - Z$ relation, but it is extremely difficult to extract. This is because the relation is affected by both flows (which may influence the metallicity, but not the luminosity) and the detailed history of star formation (which affects both metallicity and luminosity). Luminosity is a proxy for stellar mass, but how representative of stellar mass it is depends upon the bandpass.

In a series of four papers, Melbourne and Salzer (2002), Melbourne et al. (2004), Lee, Salzer, & Melbourne

(2004) and Salzer et al. (2005) studied the $L-Z$ relationship of giant “starburst emission-line galaxies” (ELGs), using data in the visible and NIR. The authors derived a linear relationship with a steeper slope than previously found for dwarfs, finding that the slope decreases as the wavelength of the luminosity bandpass increases. Using spectra of 6387 emission-line star-forming galaxies, Lamareille et al. (2004) confirmed a linear $L-Z$ relation in the local Universe ($z < 0.15$) over a large range of abundances (~ 2 dex) and luminosities (~ 9 mag). Tremonti et al. (2004) utilized SDSS imaging and spectroscopy of about 53,000 star-forming galaxies at $z \sim 0.1$, finding linear $L-Z$ relationships, although contours appear to level off at high luminosities ($M_g < -20$).

A more useful relation for studying chemical evolution is the correlation between metallicity and the gas fraction. Lee et al. (2003a) and Lee, McCall, & Richer (2003) used data in the visible to show that the oxygen abundance in dIs is tightly correlated with the gas fraction. The result was used to argue that dIs have evolved in isolation, without inflow or outflow of gas. The observations pointed to a subsolar yield (e.g., Garnett 2002), but the significance of this is difficult to assess because values for yields are critically dependent upon methods used to determine abundances. However, yields are relative, being critically dependent on methods used to determine abundances. A somewhat different conclusion was reached by van Zee and Haynes (2006), who measured abundances in 21 apparently isolated dIs selected based on their morphological classification and distances determined mostly from systemic velocities. While several galaxies in their sample follow the closed box model, they argue that either outflow of enriched gas or inflow of pristine gas has occurred in most galaxies.

1.4. NIR Imaging of Dwarfs

The utility of light as a gauge of galaxy mass depends upon the wavelength of observation. In star-forming galaxies such as dIs and most BCDs, the young population shines brightly in the visible, overwhelming the light from the old stellar component, which traces the bulk of the mass. Therefore, observations in the visible do not necessarily reflect the stellar mass of a galaxy. This problem can be reduced in the near-infrared (NIR), where the intermediate-age and old populations become more visible. Furthermore, light in the NIR is much less attenuated by extinction (absorption of light due to internal and Galactic dust) than light in the visible.

Vaduvescu et al. (2005a) (hereafter referred to as Paper I) and Vaduvescu, Richer, & McCall (2006) (hereafter referred to as Paper II) studied the structural properties of dIs and BCDs in the NIR. The dI sample (Paper I) included 28 dwarfs from the Local Volume closer than

5 Mpc having accurate distances from the literature (i.e., derived using Cepheids and the tip of the red giant branch). The BCD sample (Paper II) included 16 dwarfs in the Virgo Cluster, all approximated to have the same distance modulus ($DM = 30.62$). The surface brightness profiles of dIs were fitted using a sech law, which models the light at all radii, while BCDs were fitted using a sech function to model the diffuse old component plus a Gaussian to model the young starburst (at small radii). Absolute sech magnitudes were derived using the known distances and correcting for the extinction. These data are used here to gauge the stellar masses of the systems and thereby make possible a detailed study of chemical evolution.

1.5. The Present Paper

In the present paper, we analyse the chemical properties of our dI and BCD samples. We use the NIR data gathered in Papers I and II, in conjunction with metallicities taken from the literature and derived from our own spectra, to derive fundamental relations relevant to the formation and evolution of dwarfs and to compare dIs and BCDs chemically.

In Section 2, we present spectral observations of four Virgo BCDs which we observed at Gemini North, and in Section 3 their reduction. Sections 4 and 5 address chemical properties of dIs and BCDs, considering correlations among luminosity, metallicity, mass (in various forms), and the gas fraction. In Section 6, we approach the implications for evolution, comparing dIs and BCDs in the context of the closed box model. Section 7 presents our conclusions.

2. Gemini Observations

Using Gemini-North with GMOS, we detected $[\text{O III}]\lambda 4363$ in two of the four BCDs which we observed. Long-slit spectra of four BCDs in the Virgo Cluster (VCC 24, VCC 459, VCC 641, and VCC 2033) were acquired in queue mode on two nights between Feb 28 and Mar 2, 2003. The data were taken with the Gemini Multi-Object Spectrograph (GMOS) mounted at the $f/15.82$ focus of the Gemini-North 8.1 m telescope located atop Mauna Kea, Hawaii. The slit width was $0.5''$ and the slit length was $5.5'$. The GMOS camera includes three CCDs with 2048×4608 pixels each, creating a mosaic of 6144×4608 pixels. Pixel sizes are $13.5 \mu\text{m}$, so the scale is $0.0824''/\text{pixel}$ along the dispersion axis and $0.0727''/\text{pixel}$ along the slit axis. We used the B600-G5303 grating which gave a spectral resolution of $0.45 \text{ \AA}/\text{pixel}$. Data were acquired both in the blue (central wavelength of the grating 4680 \AA ,

range 3298-6062 Å) and in the red (central wavelength 5600 Å, range 4218-6982 Å). Data were binned 4×4 . Air masses were between 1.0 and 1.2, so the slit was not oriented along the parallactic angle.

Dome flat fields were acquired every night for all instrumental settings, interspersed between blue and red galaxy spectra, and also between blue and red standard star spectra. Biases were taken at the end of the run. One spectroscopic standard star, Feige 66, was observed once every night. We include the log of our observations in Table 1.

3. Data Analyses

3.1. Reductions

Images were reduced using the GEMINI v.1.6 GMOS package under IRAF using the sequence given in Vaduvescu (2005). Bias and flat field frames (the latter taken for each instrument setting) were applied first, then individual spectra were combined for each grating setting. The arc lamp spectra were corrected for bias and flat field and used to calibrate the combined red and blue spectra. The two-dimensional spectra were collapsed to one dimension. The same sequence was applied to the standard star spectra. Spectra were calibrated using the standard star observations, correcting for atmospheric extinction. The blue and red calibrated spectra were joined into final spectra, using the common lines $H\beta$ $\lambda 4861$, $[O III]\lambda 4959$ and $[O III]\lambda 5007$ to equalize flux scales. The scale factors ranged between 1.3 and 2.4.

Figures 1 to 3 present the reduced combined spectra of VCC 459, VCC 2033, VCC 24, and VCC 641. The first two are presented using different scalings to show the bright and faint lines. The last two show fewer lines, so they are displayed using a single scaling. In a few cases, a “fracture” due to imperfect combination of the red and blue spectra is visible in the overlapping region at 6200 Å. Because the scaling of the red and blue spectra was based entirely upon emission line fluxes, measurements of the emission lines should be unaffected.

3.2. Line Measurements

We detected $[O III]\lambda 4363$ in the core of two Virgo BCDs, namely VCC 459 and VCC 2033, for which it was possible to determine the oxygen abundances using the direct method. In VCC 24 and VCC 641 we did not detect $[O III]\lambda 4363$, but did measure stronger lines. For them, we were able to use the bright-line method to derive abundances.

Emission lines were measured using INTENS, a FORTRAN program developed by McCall, Rybski, & Shields (1985). This is a non-interactive non-linear least-squares fitting program which can efficiently fit and measure emission and/or absorption lines in one-dimensional spectra (flux versus wavelength) or two-dimensional spectra (flux versus wavelength as a function of spatial position). All spectra analyzed in this paper were one-dimensional.

A few of the hydrogen lines exhibited obvious underlying Balmer absorption, especially at $H\beta$. Using INTENS, a simultaneous fit of emission and absorption profiles allowed for a direct determination of the flux in the emission and the equivalent width of the underlying Balmer absorption. Measured emission fluxes are given in Table 2. In Figure 4, we illustrate two fits.

3.3. Abundances

We used SNAP (Spreadsheet Nebular Analysis Package; Krawchuk et al. 1997) to derive abundances from ratios of line fluxes. SNAP is an add-in for Microsoft ExcelTM. From appropriately chosen spectral diagnostics, SNAP will compute reddening, apply equivalent width and reddening corrections, compute electron temperatures and densities, and compute ionic abundances.

Using SNAP, the extinction was calculated using $F(H\alpha)/F(H\beta)$ ratio, assuming the reddening model of Fitzpatrick (1999) and that the dust is located in the Galactic foreground. The redshift of each galaxy was taken from NED. If the $[\text{O III}]\lambda 4363$ line was detected, then the temperature was calculated using $I([\text{O III}]\lambda 5007)/I([\text{O III}]\lambda 4363)$. Otherwise, the temperature was assumed to be $T_e = 10,000$ K. The electron density was computed using the $I([\text{S II}]\lambda 6716)/I([\text{S II}]\lambda 6731)$ ratio. If the $[\text{S II}]$ lines were poorly measured, a density of 100 electrons/cm³ was assumed.

Once the data were corrected for reddening, the ionic abundances of O^+ and O^{++} relative to H^+ were calculated for those objects for which $[\text{O III}]\lambda 4363$ was detected. These were then summed to get $12+\log(n(\text{O})/n(\text{H}))$.

We include in Table 2 the reddening-corrected line fluxes with respect to $H\beta$ for VCC 24, VCC 459, and VCC 2033. For VCC 641, $H\beta$ was severely affected by underlying absorption, so we report its line fluxes with respect to $H\alpha$ instead.

Table 3 lists the measured chemical properties of the four BCDs observed. For VCC 2033, $[\text{O III}]\lambda 4363$ was marginally detected, and thus, the oxygen abundance error is large (0.3 dex).

Using the bright line R_{23} method (McGaugh 1991, 1994), we derive $12 + \log(\text{O}/\text{H}) = 8.31$, which is 0.3 dex higher than the $[\text{O III}]\lambda 4363$ value ($12 + \log(\text{O}/\text{H}) = 7.99 \pm 0.30$). The R_{23} value seems to agree better with the measurement of Vilchez and Iglesias-Paramo (2003), who give lower and upper limits of 8.11 and 8.40, respectively. Due to the large error in our $[\text{O III}]\lambda 4363$ measurement, we adopt for VCC 2033 an oxygen abundance which is the average value of the $[\text{O III}]\lambda 4363$ and the R_{23} measurements, i.e., $12 + \log(\text{O}/\text{H}) = 8.15 \pm 0.15$. For VCC 641, $\text{H}\beta$ was not detected, so in this case we used the emissivity calculations to determine the ratio $\text{H}\alpha/\text{H}\beta$, then we employed the bright line method. van Zee, Skillmann, & Haynes (2006) compare the reliability of empirical and semi-empirical methods to derive abundances, suggesting that the typical error in an abundance derived from R_{23} is around 0.2 dex. We include this error for all our R_{23} results in Tables 3, 4, and 5.

4. Chemical Properties of Dwarf Galaxies

4.1. Our Luminosity-Metallicity Relation for dIs

In Table 4, we include the oxygen abundances for 17 dwarfs classified as dIs from our Local Volume sample, out of 27 observed in the NIR (Paper I), together with their sources. In the second part of the table we include four dwarfs from Virgo observed by us in the NIR (Paper II), classified as dIs based on their luminosity profiles. In the last part of the Table we append another 8 dIs with known metallicities from the literature for which K_s luminosities are determined from 2MASS data using the best distances available in the literature (Fingerhut 2005, personal communication). Note that 2MASS stars were used to derive zero-points for our observed fields (Papers I and II), so the photometric scales are consistent. Nevertheless, one must be wary of 2MASS magnitudes for galaxies, owing to the short exposure times and the correspondingly bright detection-thresholds.

In Figure 5, we plot the $L_K - Z$ relationship for the 29 dIs in Table 4. For the galaxies observed by us, we use sech absolute magnitudes, while for the ones observed by 2MASS, we use total absolute magnitudes. T_e -based abundances are plotted as solid symbols, and R_{23} -based abundances as open symbols. We include errors in metallicities; typical errors for absolute magnitudes are about 0.1 mag. There is an excellent correlation. Four outliers appear in the plot: NGC 5264 and NGC 3741, whose metallicities are derived using the bright line method, Holmberg II, whose K_s magnitude comes from 2MASS, and VCC 1725.

Following Lee et al. (2003a), a best-fit line for the correlation between two parameters with comparable errors can be obtained with the geometric mean functional relationship

(Draper and Smith 1998), which assumes similar dispersions in both observables. An equal weighting of points is assigned for both variables in a given fit. The geometric mean functional relationship relies upon the minimization of the sum of areas bounded by the shortest horizontal and vertical lines from each data point to the best-fit line.

Excluding the four labeled points, we obtain the following L_K - Z relationship for 25 dIs from Table 4:

$$12 + \log(\text{O}/\text{H}) = (-0.141 \pm 0.015)M_K + (5.581 \pm 0.244) \quad (1)$$

We plot the fit as a dashed line in Figure 5. Most of the points are consistent with the fit, given the errors in metallicities. A nearly identical relationship is obtained in J :

$$12 + \log(\text{O}/\text{H}) = (-0.140 \pm 0.014)M_J + (5.692 \pm 0.214) \quad (2)$$

The rms dispersion in abundances in the $L - Z$ relations in K_s and J is 0.11 and 0.10, respectively. Similar relations are obtained using the isophotal and total absolute magnitudes instead of the sech magnitudes.

4.2. Our Luminosity-Metallicity Relation for BCDs

In Table 5, we include 15 dwarfs classified as BCDs based on the literature and luminosity profiles. In the first part of the table, we include 12 BCDs from Virgo (Paper II), and, in the last part, the three dwarfs from the Local Volume classified as BCDs based on their luminosity profiles (Paper II) and van der Bergh (2000).

In Figure 6, we plot the $L_K - Z$ relationship for 15 BCDs from Table 5. To sample the underlying stellar population, we employed sech magnitudes. T_e -based abundances are plotted as solid points, and R_{23} -based abundances as open triangles. We include errors in metallicities; typical errors for absolute magnitudes are about 0.1 mag. One outlier appears in the plot, VCC 641, having a very uncertain oxygen abundance. Excluding this point, we obtain the following $L_K - Z$ relation for 14 BCDs from geometric mean fitting:

$$12 + \log(\text{O}/\text{H}) = (-0.224 \pm 0.030)M_K + (4.212 \pm 0.537) \quad (3)$$

We plot the fit as a dashed line in Figure 6. A similar $L_J - Z$ relationship is obtained in J :

$$12 + \log(\text{O}/\text{H}) = (-0.216 \pm 0.028)M_J + (4.530 \pm 0.473) \quad (4)$$

The rms dispersion in abundance in the $L - Z$ relations in K and J is 0.12 and 0.11, respectively. Similar relations are obtained using the isophotal and total magnitudes instead of the sech magnitudes.

In Figure 7, we combine the dIs and BCDs in our samples. For visibility reasons, we do not include the five outlier points. The solid line represents the $L_K - Z$ relation for the dIs. Recall the sech magnitude for BCDs excludes the luminosity of the starburst and so represents the underlying stellar component. Figure 7 illustrates that, though the $L_K - Z$ relations for dIs and BCDs are formally different, the two samples largely overlap. Given the relatively poor luminosity distribution of our BCD sample (M_K mostly between -18 and -20), more data are required to definitively decide whether the two $L_K - Z$ relations are really different.

4.3. Comparison with the Literature

In Table 6, we summarize different $L - Z$ relationships presented in the literature. The $L - Z$ relation we derive here for local dIs is similar to those found by others in the B -band (Skillman, Kennicutt, & Hodge 1989; Richer and McCall 1995; Lee et al. 2003a; van Zee and Haynes 2006) and in the NIR (Saviane et al. 2005). The coefficients derived by us in the NIR are very close to the ones derived by Richer and McCall (1995) and van Zee and Haynes (2006) in the visible employing mostly T_e -based abundances. Using NIR luminosities has not reduced the scatter about this relation for dIs, perhaps due to the difficulty of obtaining sufficiently deep NIR photometry. Recently, de Oliveira et al. (2006) used data from Paper I and 2MASS to find a $L_K - Z$ relation very similar to ours but with larger dispersion. Their sample includes 29 dwarfs, of which six appear to be BCDs. Lee et al. (2006) find less scatter in the $L - Z$ relation using mid-IR luminosities at 4.5 microns from the *Spitzer Space Telescope*. Assuming that most of the galaxies of Salzer et al. (2005) are BCDs and that their total magnitudes approximate the old component, then their results are in agreement with ours, provided BCDs and dIs follow different $L - Z$ relations.

The studies quoted in Table 6 may be divided into local and more distant samples of dwarf galaxies. The slopes of the $L - Z$ relations for the local samples (Skillman, Kennicutt, & Hodge 1989; Richer and McCall 1995; Lee et al. 2003a; Shi et al. 2005; de Oliveira et al. 2006; Lee et al. 2006, and this work) are all very similar. There may be a difference between the slopes in the blue and infrared, but it is slight. The more distant samples of dwarfs (Lamareille et al. 2004; Tremonti et al. 2004; Salzer et al. 2005), however, all produce $L - Z$ relations with steeper slopes, reminiscent of our relation for BCDs. If these samples of more distant dwarfs are composed primarily of BCDs with some smaller fractions of dIs, the steeper slopes make sense. However, based upon our data, it is possible that the steeper slope arises from an imperfection in the calibration of R_{23} at high metallicity.

5. Mass-Metallicity Relations

Gas-rich star forming dwarf galaxies are systems that are well mixed chemically, elemental abundances being observed to vary very little across their faces (Kobulnicky and Skillman 1996, 1997; Pagel 1997), having no significant spacial inhomogeneities in [O III] λ 4363 oxygen abundances measured from HII regions located at different galactocentric radii (Lee and Skillman 2004; Lee, Skillman, & Venn 2005, 2006). Chemical evolution can be explored via correlations between oxygen abundance and the stellar mass, gas mass, total mass, and the gas fraction.

Using data in B for a sample of dIs observed in the field, Lee et al. (2003a) showed that the oxygen abundance correlates with the stellar mass of the systems. However, in another sample of dIs in the Virgo Cluster, the relation was more scattered. Lee, McCall, & Richer (2003) found also that the relation with the gas mass was scattered for the field sample, and that some Virgo dIs were depleted in gas. The relation between metallicity and the gas fraction suggested that the evolution of some dIs in Virgo was affected by flows, such as stripping of gas due to the cluster neighborhood. The authors showed that this relationship could be used unequivocally to recognize gas deficiency in dwarfs. Below we address the relations between metallicity and mass, employing NIR photometry.

5.1. Gas Masses

The total mass of gas can be gauged from the HI 21-cm flux, F_{21} , measured by radio observations (Huchtmeier et al. 2000; Huchtmeier, Karachentsev, & Karachentseva 2001, 2003). Data for dIs are summarized by Karachentsev et al. (2004). We include in Table 4 the logarithm of the total HI flux from the latter source. For Virgo BCDs, HI fluxes are given in Table 5. They are derived from Gavazzi et al. (2005), who synthesize a set of data for 355 late-type galaxies in the Virgo cluster with HI masses for many dwarfs derived from previous work by Hoffman and collaborators (Huchtmeier et al. 2000; Huchtmeier, Karachentsev, & Karachentseva 2001, 2003).

The HI mass, M_{HI} , in solar masses is given by the following equation (Roberts 1975; Roberts and Haynes 1994):

$$M_{HI} = 2.356 \times 10^5 F_{21} D^2 \quad (5)$$

where F_{21} is the 21-cm flux integral in Jy km s^{-1} and D is the distance in Mpc. To account for helium and other metals, the total gas mass in solar masses is given by

$$M_{gas} = M_{HI}/X \quad (6)$$

where X is the fraction of the gas in the form of hydrogen, here assumed to be 0.733 (Lee et al. 2003a). In Table 4 we include the logarithm of the total gas mass for the dIs in our sample, calculated from F_{21} and the distance modulus included in the first column. In Table 5 we include the logarithm of the total gas mass for the BCDs in our sample.

Figure 8 plots the metallicity versus the logarithm of the total gas mass (expressed in solar units). dIs are plotted with circles, and BCDs with triangles. Dwarfs having T_e abundances are plotted with solid symbols and those having R_{23} abundances with open symbols. The correlation for the dIs is very poor, with NGC 5264 again being an outlier in the sample. Rejecting this point, a geometric linear fit to the rest of the dI sample (28 objects) gives the following relation:

$$12 + \log(\text{O}/\text{H}) = (5.13 \pm 0.45) + (0.34 \pm 0.06) \log(M_{\text{gas}}) \quad (7)$$

This relation is very close to the fit found by Lee et al. (2003a), who used data for 21 dIs. The two samples overlap, with the sample of Lee et al. (2003a) extending from $M_B = -18$ to -11 mag (corresponding to M_K from -21 to -14), and our sample extending from $M_K = -20$ to -13 . We plot in Figure 8 our fit with a solid line and the fit of Lee et al. (2003a) with a dotted line. Some Virgo BCDs lie leftward of the dI envelope, i.e., less gas for a given oxygen abundance, a result found also in Lee, McCall, & Richer (2003) for their Virgo dI sample, suggesting that they are depleted in gas relative to dIs of comparable metallicity. Either they are less massive systems overall, or gas has been removed, perhaps by dynamical interactions in the cluster environment.

5.2. Stellar Masses

In Paper I, it was shown that the shape of the unresolved (diffuse) stellar component of nearby dIs in the NIR is approximated well by a hyperbolic secant (sech) function. In Paper II, it was demonstrated that the same function fits the shape of the diffuse component underlying star formation bursts in BCDs. It is believed that the luminosity associated with the sech model provides a good estimate of the contribution to the light by stellar populations older than about 3 Gyr (Paper I). As such, it should be the best gauge of total stellar mass.

Expressed in solar masses, stellar masses can be calculated from

$$\log M_* = \log \frac{M_*}{L_K}(\text{old}) - 0.4(M_K(\text{old}) - M_{K\odot}) \quad (8)$$

where $M_*/L_K(\text{old})$ is the mass-to-light ratio of the old stellar component in K_s , in solar units, $M_K(\text{old})$ is the absolute magnitude of the old component in K_s , and $M_{K\odot}$ is the absolute

magnitude of the Sun in K_s . Here, we prefer the sech magnitudes derived in Papers I and II as representative of the luminosity of the old population, $M_K(old)$. However, we augment the dI sample with galaxies detected by 2MASS for which catalogued total magnitudes are used as estimates of $M_K(old)$. These galaxies are distinguished symbolically in plots. For the absolute magnitude of the Sun, we adopt $M_{K\odot} = +3.3$ (Bessell, Castelli, & Plez 1998).

For low metallicity galaxies ($0.004 Z_\odot$ to $0.0004 Z_\odot$), Portinari (2005, private communication) derived $M_*/L_K \sim 0.8 M_\odot/L_{K\odot}$ using population synthesis models. Drory et al. (2004) obtained an identical result from composite stellar population models for ages between about 4 and 8 Gyr (see their Figure 1). From extensive modeling of the Milky Way, Bissantz, Englmaier, & Gerhard (2003) derived $M_*/L_K = 0.6$. Based on galaxy evolution models to investigate the relation between mass to light ratios and colours of spiral galaxies, de Jong and Bell (2003) predict $M/L_K \sim 1 M_\odot/L_{K\odot}$ for $B - R \sim 2$ mag (which can be regarded as an average colour of dwarfs). Here, we adopt $M_*/L_K = 0.8 M_\odot/L_{K\odot}$.

5.3. Baryonic Masses

Assuming baryonic matter consists of gas and stars only, the baryonic mass of a galaxy can be expressed simply by the sum of the two components, $M_{bary} = M_{gas} + M_*$. Figure 9 plots the metallicity versus the logarithm of the baryonic mass expressed in solar masses. dIs are plotted with circles, and BCDs with triangles. Dwarfs having T_e abundances are plotted with solid symbols, while those having R_{23} abundances with open symbols. In the dI sample, NGC 5264 is once more an outlier. Rejecting this point, a geometric linear fit to the rest of the sample (28 dIs) gives the following relation:

$$12 + \log(\text{O}/\text{H}) = (4.91 \pm 0.46) + (0.35 \pm 0.05) \log(M_{\text{bary}}) \quad (9)$$

This relation is very close to the fit found by Lee et al. (2003a) which was derived from B photometry for 21 dIs in the field. We plot our fit with a solid line and the fit of Lee et al. (2003a) with a dotted line. The close agreement suggests that the two-component decomposition scheme of (Lee et al. 2003a) was effective for deriving stellar masses. Most BCDs in Figure 9 appear to lie at lower baryonic masses compared to dIs at a given oxygen abundance, possibly as a consequence of how BCDs are selected. It is possible that larger galaxies with comparable bursts are simply not classified as BCDs!

5.4. Metallicity and Gas Fraction

The closed box model of chemical evolution predicts a linear correlation between $n(\text{O})/n(\text{H})$ and the logarithm of the inverse gas fraction $1/\mu$, where

$$\mu = \frac{M_{gas}}{M_{gas} + M_*} \quad (10)$$

The slope of the relation conveys the yield of oxygen. Judging stellar masses from BV photometry, Lee et al. (2003a) concluded that field dIs obey the closed box model, implying that their evolution has been isolated. Here, we study the correlation obtained for both dIs and BCDs using NIR sech luminosities to assess stellar masses. In principle, our masses should be more reliable, as they are less sensitive to recent star formation.

Figure 10 plots $\log(\text{O}/\text{H})$ versus $\log(\log(1/\mu))$, for which the closed box model predicts a linear correlation with a slope of unity and an intercept equal to the yield. Gas fraction μ increases to the left, according to the labels plotted along the top horizontal axis. We represent dIs with photometry from the present work with circles, and dIs with 2MASS photometry with crosses. We plot the fit of Lee et al. (2003a) with a dotted line. Most dIs from our sample lie close to the fit of Lee. We overlay in Figure 10 triangles representing our BCD sample. Most BCDs appear close to the fit of Lee, too, with about three outliers. Note that gas has not been detected in VCC 802, so its abscissa is a lower limit. One possibility is that VCC 802 has been stripped due to the hot intracluster medium since it is projected near the M86/M84 clump, which is a region of enhanced density (Boehringer et al. 1994). If dIs follow the closed box model, as the data suggests, then the proximity of BCDs to the dI locus suggests that bursts in present-day BCDs do not have sufficient strength to blow out neutral gas from the host galaxies. The fact that several dIs and at least one BCD do show HI deficiencies in dense environments (Lee et al. 2003a; this paper) indicates that external processes are more likely to remove gas from dwarfs. In summary, we concur with Lee that the evolution of field dIs has not been affected much by flows. We also conclude that BCDs have evolved similarly to dIs.

6. Implications for Evolution

A few evolutionary scenarios that involve dIs and BCDs have been proposed over the years, most without firm conclusions (e.g., Papaderos et al. 1996b). Some links have emerged using stellar masses derived from data in the visible, although with large scatter. We summarize below our main results.

For both dIs and BCDs, metallicity correlates with stellar mass, gas mass, and baryonic

mass, in the sense that more massive systems are more enriched in metals. Our most important discovery is that the relationship between the metallicity and the gas fraction for BCDs follows that for dIs. It means that BCDs and dIs have evolved similarly. Using NIR photometry, we confirm the conclusion of Lee et al. (2003a) that the evolution of field dIs has not been noticeably influenced by gas flows. By implication, the same conclusion must be reached for BCDs. Thus, star formation bursts in BCDs are unlikely to be caused by the transfer of material from elsewhere.

7. Conclusions

Oxygen abundances have been derived for four blue compact dwarf galaxies in the Virgo Cluster observed in a queue run at Gemini-North in 2003. Drawing upon the NIR properties studied in Papers I and II and oxygen abundances from our work and the literature, we studied the correlations between the metallicity and the stellar mass, gas mass, baryonic mass, and the gas fraction for both dIs and BCDs. Metallicity correlates with all four parameters, in the sense that more massive systems contain more metals. The oxygen abundance correlates well with the luminosity in K_s , for both dIs and BCDs. Using NIR sech magnitudes to measure luminosity, the $L_K - Z$ relations for dIs and BCDs are statistically indistinguishable. dIs and BCDs appear to share a common relationship between metallicity and the gas fraction, namely one which is consistent with the closed-box evolution. Thus, BCDs appear to be dIs with enhanced star formation activity. The origin of the enhancement remains unknown, but it is unlikely to be caused by flows.

We thank the Gemini-North time allocation committees for granting us the opportunity to observe. MLM thanks the Natural Sciences and Engineering Research Council of Canada for its continuing support. MGR acknowledges financial support from CONACyT grant 43121 and UNAM DGAPA grants IN108406-2, IN108506-2, and IN112103. OV thanks Dr. Henry Lee for providing up-to-date references regarding metallicities. Special acknowledgement is due to Dr. Jose Manuel Vilchez who served as the external examiner for the PhD thesis of OV, providing interesting discussions. Thanks are due to Robin Fingerhut for providing updated distances of dwarfs in the Local Volume. For our data reductions, we used the GEMINI package written at the Gemini Observatories and IRAF, which is maintained by the National Optical Astronomy Observatories, operated by the Association of Universities for Research in Astronomy, Inc., under cooperative agreement with the National Science Foundation. This research has made use of the GOLDMine Database in Milano and the NASA/IPAC Extragalactic Database (NED) which is operated by the JPL, CALTECH, under contract with NASA. Special acknowledgement is due to an anonymous referee who

provided discussions which allowed us to improve the manuscript.

REFERENCES

- Allende Prieto, C., Lambert, D. L., & Asplund, M., 2001, *ApJ*, 556, L63
- Bessell, M. S., Castelli, F., & Plez, B., 1998, *A&A*, 333, 231
- Binggeli, B., 1994, A Note on the Definition and Nomenclature of Dwarf Galaxies, in *Dwarf Galaxies*, ESO Conference and Workshop Proc No. 49, Eds. G. Meylan and P. Prugniel, Paris, p. 13
- Bissantz, N., Englmaier, P., & Gerhard, O., 2003, *MNRAS*, 340, 949
- Boehringer, M., Briel, U. G., Schwarz, R. A., Voges, W., Hartner, G., Trumper, J., 1994, *Nature*, 368, 828
- de Jong, R. S. and Bell, E. F., 2003, Stellar M/L Ratios and Spiral Galaxy Dynamics, in *The Mass of Galaxies at Low and High Redshift*, Proceedings of the ESO and Universitäts-Sternwarte Munchen Workshop, Venice, Italy, 24-26 Oct 2001, ESO Astrophysics Symposia, Eds. Bender, R. and Renzini, A., Springer-Verlag, 2003, p. 213
- de Oliveira, M., Temporin, S., Cypriano, E. S., Plana, H., Amram, P, Sodre, L. Jr., Balkowski, C., 2006, *AJ*, 132, 570
- Draper, N. R. and Smith, H., 1998, *Applied Regression Analysis*, New York: Wiley, p. 89
- Drory, N., Bender, R., Feulner, G., Hopp, U., Maraston, C., Snigula, J., Hill, G. J., 2004, *ApJ*, 608, 742
- Fitzpatrick, E. L., 1999, *PASP*, 111, 63
- Gallagher, G. and Hunter, D. A., 1989, *AJ*, 98, 806
- Garnett, D. R., 2002, *ApJ*, 581, 1019
- Gavazzi, G., Boselli, A., van Driel, W., O’Neil, K., 2005, *A&A*, 429, 439
- Grebel, E. K., 2000, The Local Group, in *Microlensing 2000: A New Era of Microlensing Astrophysics*, ASP Conf. Ser., Eds. J. W. Menzies and P. D. Sackett, cape Town, also in astro-ph/0008249
- Grebel, E. K., 2001, *ApJS*, 277, 231

- Guseva, N. G., Izotov, Y. I., & Thuan, T. X., 2000, *ApJ*, 531, 776
- Helmi, A. et al., 2006, *ApJ*, 651L, 121
- Hidalgo-Gamez, A. M. and Olofsson, K., 1998, *A&A*, 334, 45
- Hidalgo-Gamez, A. M., Sanchez-Salcedo, F. J., & Olofsson, K., 2003, *A&A*, 399, 63
- Hodge, P. and Miller, B. W., 1995, *ApJ*, 451, 176
- Huchtmeier, W. K. and Richter, O.-G., 1989, *A General Catalog of HI Observations of Galaxies. The Reference Catalog*, Berlin: Springer-Verlag
- Huchtmeier, W. K., Karachentsev, I. D., Karachentseva, V. E., Ehle, M., 2000, *A&A*, 141, 469
- Huchtmeier, W. K., Karachentsev, I. D., & Karachentseva, V. E., 2001, *A&A*, 377, 801
- Huchtmeier, W. K., Karachentsev, I. D., & Karachentseva, V. E., 2003, *A&A*, 401, 483
- Hunter, D. A. and Hoffman, L., 1999, *AJ*, 117, 2789
- Izotov, Y. I. and Thuan, T. X., 1999, *ApJ*, 511, 639
- James, P. A., 1994, *MNRAS*, 269, 176
- Karachentsev, I. D., Karachentseva, V. E., Huchtmeier, W. K., Makarov, D. I., 2004, *AJ*, 127, 2031
- Kauffmann, G., White, S. D. M., & Guiderdoni, B., 1993, *MNRAS*, 264, 201
- Kennicutt, R. C. and Skillman, E. D., 2001, *AJ*, 121, 1461
- Kobulnicky, H. A. and Skillman, E. D., 1996, *ApJ*, 471, 211
- Kobulnicky, H. A. and Skillman, E. D., 1997, *ApJ*, 489, 636
- Krawchuk, C. A. P., McCall, M. L., Komljenovic, M., Kingsburgh, R., Richer, M., Stevenson, C., 1997, SNAP: Spreadsheet nebular analysis package, *Planetary Nebulae, IAU Symposium 180*, Eds. H. J. Habing and G. L. M. Lamers, Dordrecht: Kluwer Academic Publishers, p. 116
- Kunth, D. and Ostlin, G., 2000, *The Most Metal-Poor Galaxies*, *The Astronomy and Astrophysics Review*, 10, Issue 1/2, p. 1-79

- Lamareille, F., Mouhcine, M., Contini, T., Lewis, I., Maddox, S., 2004, MNRAS, 350, 396
- Lee, J., Salzer, J. J., & Melbourne, J., 2004, ApJ, 616, 752
- Lee, H., McCall, M. L., Kingsburgh, R. L., Ross, R., Stevenson, C., 2003, AJ, 125, 146
- Lee, H., McCall, M. L., & Richer, M. G., 2003, AJ, 125, 2975
- Lee, H., Grebel, E. K., & Hodge, P. W., 2003, ApJ, 401, 141
- Lee, H. and Skillman E. D., 2004, ApJ, 614, 698
- Lee, H., Skillman E. D., & Venn, K. A., 2005, ApJ, 620, 223
- Lee, H., Skillman, E. D., Cannon, J. M., Jackson, D. C., Gehrz, R. D., Polomski, E. F., Woodward, C. E., 2006, ApJ, 647, 970
- Lee, H., Skillman E. D., & Venn, K. A., 2006, ApJ, 642, 813
- Lequeux, J., Peimbert, M., Rayo, J. F., Serrano, A., Torres-Peimbert, S., 2003, A&A, 80, 155
- Martin, C. L., 1997, ApJ, 491, 561
- Mateo, M., 1998, ARA&A, 36, 453
- Matthews, L. D. and Gallagher, J. S., 1997, AJ, 114, 5
- McCall, M. L., Rybski, P. M., & Shields, G. A., 1985, ApJS, 57, p. 1-62
- McGaugh, S. S., 1991, ApJ, 426, 135
- McGaugh, S. S., 1994, ApJ, 380, 140
- Melbourne, J. and Salzer, H. J., 2002, AJ, 123, 2302
- Melbourne, J., Phillips, A. S., John J., Gronwall, C., Sarajedini, V. L., 2004, AJ, 127, 686
- Miller, B. W. and Hodge, P., 1996, ApJ, 458, 467
- Moles, M., Aparicio, A., & Masegosa, J., 1990, A&A, 228, 310
- Osterbrock, D. E., 1989, *Astrophysics of Gaseous Nebulae and Active Galactic Nuclei*, Sausalito: University Science Books
- Papaderos, P., Loose, H.-H., Thuan, T. X., Fricke, K. J., 1996a, A&AS, 120, 207

- Papaderos, P., Loose, H.-H., Fricke, K. J., Thuan, T. X., 1996b, *A&A*, 314, 59
- Pagel, B. E. J., Edmunds, M. G., Blackwell, D. E., Chun, M. S., Smith, G., 1979, *MNRAS*, 189, 95
- Pagel, B. E. J., 1997, *Nucleosynthesis and the Chemical Evolution of Galaxies*, Cambridge: Cambridge Univ. Press
- Pena, M. and Ayala, S., 1993, *Rev. Mexicana Astron. Astrofis.*, 27, 171
- Peimbert, M., Peimbert, A., Esteban, C., Garcia-Rojas, J., Bresolin, F., Carigi, L., Ruiz, M. T., Lopez-Sanchez, A. R., 2006, *The Calibration of the O/H Abundance Indicators for Extragalactic HII regions based on OII Recombination Lines*, in *First Light Science with the Gran Telescopio Canarias*, to appear in *Rev. Mexicana Astron. Astrofis.(SC)*, astro-ph/0608440
- Pilyugin, L. S., 2000, *A&A*, 362, 325
- Pilyugin, L. S., 2001, *A&A*, 369, 594
- Pilyugin, L. S., 2001, *A&A*, 374, 412
- Pilyugin, L. S., Vilchez, J. M., & Contini, T., 2004, *A&A*, 425, 849
- Richer, M. G. and McCall, M. L., 1995, *ApJ*, 445, 642
- Roberts, M. S., 1975, *Radio Observations of Neutral Hydrogen in Galaxies*, in *Galaxies and the Universe*, Eds. A. Sandage, M. Sandage and J. Kristian (Chicago: University of Chicago Press), p. 309
- Roberts, M. S. and Haynes, M. P., 1994, *ARA&A*, 32, 115
- Salzer J. J., Lee, J. C., Melbourne, J., Hinz, J. L., Alonso-Herrero, A., Jangren, A., 2005, *ApJ*, 624, 661
- Saviane, I., Held, E. V., Ivanov, V., Alloin, D., Bresolin, F., Rich, R. M., Rizzi, L., Momany, Y., 2005, *The near-IR luminosity-metallicity relation of dwarf irregular galaxies*, in *Near-Field Cosmology with Dwarf Elliptical Galaxies, IAU Colloquium 198 Les Diablerets*, Switzerland, 14-18 March 2005, Eds. H. Jerjen and B. Binggeli
- Searle, L. and Sargent, W. L. W., 1972, *ApJ*, 173, 25
- Shi, F., Kong, X., Li, C., Cheng, F. Z., 2005, *A&A*, 437, 849

- Skillman, E. D., Kennicutt, R. C., & Hodge, P. W., 1989, *ApJ*, 347, 875
- Skillman, E. D., Terlevich, R. J., Kennicutt, R. C., Garnett, D. R., Terlevich, E., 1994, *ApJ*, 431, 172
- Sparke, L. and Gallagher, J. S., 2000, *Galaxies in the Universe: An Introduction*, Cambridge Univ. Press
- Stasinska, G., Comte, G., & Vigroux, L., 1986, *A&A*, 154, 352
- Stavely-Smith, L., Davies, R. D., & Kinman, T. D., 1992, *MNRAS*, 258, 334
- Tammann, G. A., 1994, Dwarf Galaxies in the Past, in *Dwarf Galaxies, ESO Conference and Workshop Proc No. 49*, Eds. G. Meylan and P. Prugniel, Paris, p. 3
- Thuan, T. X., 1985, *ApJ*, 299, 881
- Tremonti, C. A. et al. 2004, *AJ*, 613, 898
- Tully, R. B., Boesgaard, A. M., Dyck, H. M., Schempp, W. V., 1981, *ApJ*, 246, 38
- van den Bergh, S., 2000, in *The Galaxies of the Local Group*, Cambridge: Cambridge University Press
- van Zee, L., Haynes, M. P., & Salzer, J. J., 1997, *AJ*, 114-6, 2497
- van Zee, L., Skillman, E., & Haynes, M. P., 2006, *ApJ*, 637, 269
- van Zee, L., and Haynes, M. P., 2006, *ApJ*, 636, 214
- Vilchez, J. M. and Iglesias-Paramo, J., 2003, *ApJS*, 145, 225
- Vaduvescu, O., 2005, *Infrared Properties of Star Forming Dwarf Galaxies*, PhD Thesis, York University
- Vaduvescu, O., McCall, M. L., Richer, M. G., Fingerhut, R. L., 2005 (Paper I), *AJ*, 130, 1593
- Vaduvescu, O., Richer, M. G., & McCall, M. L., 2006 (Paper II) *AJ*, 131, 1318
- Venn, K. A., Irwin, M., Shetrone, M. D., Tout, C. A., Hill, V., & Tolstoy, E., 2004, *AJ*, 128, 117
- Webster, B. L. and Smith, M. G., 1983, *MNRAS*, 204, 743

White, S. D. M. and Frenk, C. S., 1991, ApJ, 379, 52

Table 1. Gemini-North observing log

Galaxy	α	δ	PA	Date	λ_c	Exposure
(1)	(h m s)	(deg ' ")	(deg)	(UT)	(Å)	(no.exp \times s)
	(2)	(3)	(4)	(5)	(6)	(7)
VCC 24	12:10:35.7	+11:45:38	147	Mar 1, 2003	4680	3×600
...	147	Mar 1, 2003	5600	3×200
VCC 459	12:21:12.1	+17:38:21	111	Mar 1, 2003	4680	3×600
...	111	Mar 1, 2003	5600	3×200
VCC 641	12:23:28.6	+05:48:59	15	Mar 1, 2003	4680	3×600
...	15	Mar 1, 2003	5600	3×200
VCC 2033	12:46:04.5	+08:28:33	14	Mar 2, 2003	4680	3×600
...	14	Mar 2, 2003	5600	3×200

Note. — (1) Designation of galaxy in Virgo Cluster Catalog (VCC) (2) Right Ascension (J2000) for the centre of the slit (3) Declination (J2000) for the centre of the slit (4) Slit position angle (E of N) (5) Observing date (6) Central wavelength (7) Exposure time

Table 2. Observed and corrected line ratios

Identification (Å)	VCC 24 ^a		VCC 459 ^a		VCC 641 ^b		VCC 2033 ^a	
	<i>F</i>	<i>I</i>	<i>F</i>	<i>I</i>	<i>F</i>	<i>I</i>	<i>F</i>	<i>I</i>
[O II] 3727	334.8±16.1	344.8±16.8	212.4±1.4	230.2±4.6	280.7±48.2	297.3±52.6	436.3±4.4	447.0±4.6
[H 12]	1.8±1.2	2.0±1.4
[H 11] 3771	2.3±0.3	2.5±0.3
[H 10] 3798	3.5±0.3	3.8±0.4
[He I] 3820	0.6±0.3	0.6±0.3
[H 9] 3835	4.3±0.3	4.7±0.4
[Ne III] 3869	28.3±0.6	30.3±1.0
He I + H 8 3889	15.7±0.5	16.9±0.7
[Ne III] 3967	20.2±0.4	21.5±0.6
[S II] 4069	2.0±0.3	2.1±0.3
Hδ 4101	22.3±0.3	23.6±0.6
Hγ 4340	45.3±0.4	47.1±0.9	47.0±2.0	47.5±2.1
[O III] 4363	2.8±0.3	3.0±0.4	2.1±0.9	2.1±0.9
[He I] 4472	3.5±0.1	3.6±1.5
Hβ 4861	100.0±2.1	100.0±4.3	100.0±0.5	100.0±1.0	100.0±2.8	100.0±3.0
He I 4922	1.0±0.4	1.0±0.5
[O III] 4959	92.2±3.8	92.0±4.0	132.3±1.7	131.3±2.3	54.9±6.6	56.5±7.3	57.8±1.9	57.6±2.0
[O III] 5007	271.3±8.0	270.2±8.3	396.5±2.0	392.1±3.7	82.3±11.5	84.5±12.6	172.8±3.8	172.2±3.9
[He I] 5876	12.4±0.1	11.6±0.1	13.8	13.9±4.6±0.5	9.0±0.6	9.0±0.7
[O I] 6300	4.5±0.1	4.2±0.1
[S III] 6312	1.6±0.1	1.4±0.1
[O I] 6363	1.2±0.1	1.1±0.1
[N II] 6548	16.8±2.4	16.3±2.5	7.5±0.9	6.9±0.8	7.6±1.2	7.4±1.3
Hα 6563	373.9±4.0	286.3±4.4	314.6±1.2	286.3±0.6	100.0±8.3	100.0±9.1	261.4±5.1	254.1±5.3
[N II] 6583	44.6±2.8	43.1±3.0	22.2±0.9	20.2±0.8	18.3±3.3	18.3±3.6	24.6±1.4	23.9±1.5
[He I] 6678	4.6±1.0	4.4±1.0	3.6±0.1	3.3±0.1	2.6±0.2	2.5±0.2
[S II] 6716	65.6±2.5	63.2±2.6	26.6±0.1	24.1±0.1	34.7±3.6	34.6±3.9	28.5±0.6	27.6±0.7
[S II] 6730	50.0±2.8	48.2±3.0	19.4±0.1	17.6±0.1	21.3±2.8	21.3±3.1	19.7±0.5	19.1±0.5

Note. — ^a Flux ratios are reported with respect to Hβ (Hβ=100) ^b Flux ratios are reported with respect to Hα (Hα=100). Wavelengths are listed in Å. *F* is the observed flux ratio. *I* is the flux ratio corrected for reddening.

Table 3. Derived properties for HII regions in Virgo BCDs

Property	VCC 24	VCC 459	VCC 641	VCC 2033
$I(H\beta)$ (ergs s ⁻¹ cm ⁻²)	(3.65±0.08) ×10 ⁻¹⁵	(2.38±0.07) ×10 ⁻¹⁴	...	(3.62±0.05) ×10 ⁻¹⁵
τ_1	0.032	0.087	0.028	0.026
$W(H\beta)$ (Å)	4.73±0.10	92.80±1.19	...	11.10±0.17
n_e (cm ⁻³)	...	52
log R_{23}	0.849	0.877	1.097	0.830
log O_{32}	0.021	2.273	-0.324	-0.289
$T_e(O^{+2})$ (K)	...	10500	...	12500
O^+/H^+	...	(6.9±1.4)×10 ⁻⁵	...	(6.9±0.7)×10 ⁻⁵
O^{+2}/H^+	...	(1.2±0.3)×10 ⁻⁴	...	(2.9±1.3)×10 ⁻⁵
12 + log(O/H) [T_e]	...	8.27±0.09	...	7.99±0.30
12 + log(O/H) [R_{23}]	8.58±0.20	8.09±0.20	8.86±0.20	8.31±0.20

Note. — $I(H\beta)$ represents the $H\beta$ intensity, in ergs s⁻¹ cm⁻², corrected for underlying Balmer absorption and reddening; τ_1 is the optical depth of dust at 1 μm , assuming a Fitzpatrick (1999) reddening model and dust in the foreground located in the Milky Way, calculated using $H\alpha/H\beta$; $W(H\beta)$ is the emission equivalent width, in Å, corrected for underlying Balmer absorption; n_e is the electron density; log(R_{23}) and log(O_{32}) are the diagnostics for the bright-line method (Pagel et al. 1979, McGaugh 1994); $T_e(O^{+2})$ is the computed electron temperature in degrees Kelvin; 12 + log(O/H) [T_e] is the derived oxygen abundance in dex measured via T_e ; 12 + log(O/H) [R_{23}] is the derived oxygen abundance in dex measured via R_{23} .

Table 4. Properties of the dl sample

Galaxy (1)	DM (2)	M_K (3)	$\log F_{21}$ (4)	$\log M_{gas}$ (5)	$\log M_*$ (6)	μ (7)	$12+\log(\text{O}/\text{H})$ (8)	Method (9)	Reference (10)
Cassiopeia 1	27.59	-18.23	1.70	8.24	8.51
MB 1	27.59	-17.56	0.91	7.45	8.25
UGCA 92	26.20	-15.68	2.02	8.01	7.49	0.765	7.70 ± 0.20	R_{23}	HM95
Orion dwarf	28.66	-17.96	1.89	8.86	8.41	0.740	7.88 ± 0.20	R_{23}	LFM05
DDO 47	28.39	-15.04	1.88	8.74	7.24	0.970	7.85 ± 0.04	T_e	SKH89
UGC 4115	28.53	-16.60	1.32	8.24	7.86	0.704	7.81 ± 0.20	R_{23}	LFM05
DDO 53	27.58	-13.59	1.14	7.68	6.66	0.913	7.62 ± 0.05	T_e	SKH89
UGC 4483	27.37	-14.67	1.13	7.58	7.09	0.757	7.51 ± 0.03	T_e	STK94
UGC 4998	29.95	-18.53
UGC 5423	28.11	-16.17	0.58	7.33	7.69	0.304	7.98 ± 0.10	T_e	MH96
UGC 5692	27.83	-17.62
UGC 5848	29.70	-18.11
UGC 5979	30.55	-18.49
UGC 6456	28.03	-15.50	1.15	7.87	7.42	0.736	7.64 ± 0.10	T_e	TBD81
Markarian 178	27.78	-16.04	0.48	7.10	7.64	0.224	7.82 ± 0.06	T_e	GIT00
NGC 3741	27.24	-15.02	1.72	8.12	7.23	0.886	8.10 ± 0.20	R_{23}	GH89
NGC 4163	27.30	-16.34	0.98	7.41	7.76
NGC 4190	27.20	-16.47	1.37	7.76	7.81
Markarian 209	28.37	-15.67	1.00	7.85	7.49	0.698	7.77 ± 0.01	T_e	IT99
NGC 4789A	27.80	-15.63	2.16	8.79	7.47	0.953	7.67 ± 0.05	T_e	KS01
GR 8	26.52	-13.60	0.89	7.00	6.66	0.687	7.63 ± 0.10	T_e	MAM90
DDO 167	27.93	-14.56	0.66	7.34	7.05	0.662	7.66 ± 0.03	T_e	SKH89
UGC 8508	26.87	-15.43	1.15	7.40	7.39	0.506	7.89 ± 0.20	R_{23}	LFM05
NGC 5264	28.11	-18.64	1.09	7.84	8.68	0.127	8.64 ± 0.20	R_{23}	LGH03
Holmberg IV	29.22	-18.19	1.30	8.49	8.50
DDO 187	26.78	-14.33	1.08	7.30	6.95	0.688	7.69 ± 0.09	T_e	LMK03
VCC 428	30.62	-15.78	-0.20	7.55	7.53	0.512	7.64 ± 0.09	T_e	VP03
VCC 1374	30.62	-18.17	0.40	8.15	8.49	0.315	8.35 ± 0.14	T_e	VP03
VCC 1699	30.62	-18.90	0.79	8.54	8.78	0.366	8.32 ± 0.06	T_e	VP03
VCC 1725	30.62	-18.81	0.28	8.03	8.75	0.162	7.74 ± 0.14	T_e	VP03
NGC 55	25.94	-19.69	3.43	9.31	9.10	0.621	8.34 ± 0.10	T_e	WS83
NGC 1560	27.07	-18.25	2.65	8.98	8.52	0.743	> 7.97	T_e	LMK03
Holmberg II	27.50	-18.72	2.56	9.07	8.71	0.694	7.71 ± 0.13	T_e	LMK03
NGC 3109	25.72	-16.46	3.22	9.01	7.81	0.942	7.74 ± 0.33	T_e	LMK03
IC 2574	27.86	-17.15	2.65	9.30	8.08	0.943	8.09 ± 0.07	T_e	MH96
NGC 4214	28.25	-20.34	2.51	9.32	9.36	0.476	8.24 ± 0.12	T_e	KS96
NGC 5408	27.76	-16.39	1.81	8.42	7.78	0.814	8.01 ± 0.02	T_e	SCV86
NGC 6822	23.46	-16.83	3.38	8.27	7.95	0.674	8.11 ± 0.11	T_e	L05

Note. — (1) Galaxy name, ordered by right ascension. The first two groups list our field and Virgo observed samples, and the third group lists the 2MASS sample (2) Distance modulus (3) Absolute magnitude in K_s (sech for our sample, total for 2MASS) (4) Logarithm of the total HI flux in Jy km s^{-1} (Karachentsev et al. 2004) (5) Logarithm of the total gas mass in solar masses (6) Logarithm of the stellar mass in solar masses (7) Gas fraction (8) Oxygen abundance and uncertainty (9) Method of determining abundances: T_e -direct determination via $[\text{O III}]\lambda 4363$ (Osterbrock 1989); R_{23} -determination via the bright line method (McGaugh 1994) (10) Refer-

ence for abundance: KS97: Kobulnicky and Skillman (1997); HM95: Hodge and Miller (1995); LFM05: Lee, Fingerhut and McCall, 2005 (in progress); SKH89: Skillman, Kennicutt, & Hodge (1989); STK94: Skillman et al. (1994); MH96: Miller and Hodge (1996); TBD81: Tully et al. (1981); GIT00: Guseva, Izotov, & Thuan (2000); M97: Martin (1997); GH89: Gallagher and Hunter (1989); IT89: Izotov and Thuan (1999); KS01: Kennicutt and Skillman (2001); MAM90: Moles, Aparicio, & Masegosa (1990); LGH03: Lee, Grebel, & Hodge (2003); LMK03: Lee et al. (2003a); WS83: Webster and Smith (1983); KS96: Kobulnicky and Skillman (1996); SKV86: Stasinska, Comte, & Vigroux (1986); L05: Lee, H., Skillman, E. D., & Venn, K. A., 2005, private communication; VP03: Vilchez and Iglesias-Paramo (2003)

Table 5. Properties of the BCD sample

Galaxy (1)	DM (2)	M_K (3)	$\log F_{21}$ (4)	$\log M_{gas}$ (5)	$\log M_*$ (6)	μ (7)	$12+\log(O/H)$ (8)	Method (9)	Reference (10)
VCC 24	30.62	-17.54	0.58	8.33	8.24	0.553	8.27 ± 0.20	R_{23}	V05
VCC 144	30.62	-17.73	0.36	8.11	8.31	0.387	8.35 ± 0.07	T_e	VP03
VCC 213	30.62	-19.42	0.17	7.92	8.99	0.079	8.70 ± 0.20	R_{23}	VP03
VCC 324	30.62	-18.70	0.36	8.11	8.70	0.205	8.50 ± 0.10	R_{23}	VP03
VCC 334	30.62	-17.38	0.12	7.87	8.17	0.335	8.15 ± 0.05	R_{23}	VP03
VCC 459	30.62	-18.17	0.39	8.14	8.49	0.310	8.27 ± 0.09	T_e	V05
VCC 641	30.62	-17.25	0.05	7.81	8.12	0.325	8.86 ± 0.20	R_{23}	V05
VCC 802	30.62	-16.40	< -1.13	6.62	7.78	0.065	7.84 ± 0.15	T_e	VP03
VCC 848	30.62	-17.91	0.75	8.51	8.39	0.568	8.03 ± 0.16	T_e	VP03
VCC 1313	30.62	-15.07	0.01	7.76	7.25	0.765	7.77 ± 0.06	T_e	VP03
VCC 1437	30.62	-18.37	0.40	8.15	8.57	0.277	8.30 ± 0.20	R_{23}	VP03
VCC 2033	30.62	-17.91	-0.38	7.37	8.39	0.088	8.15 ± 0.15	$T_e + R_{23}$	V05
NGC 1569	26.37	-18.19	1.87	8.05	8.49	0.268	8.19 ± 0.04	T_e	KS97
NGC 3738	28.27	-18.59	1.34	8.28	8.64	0.305	8.23 ± 0.01	T_e	M97
IC 10	24.35	-18.90	2.98	8.36	8.78	0.276	8.19 ± 0.14	T_e	LMK03

Note. — (1) Galaxy name, ordered by number. The first group represents our Virgo observed sample, and the second our BCD field sample (2) Distance modulus (3) Sech absolute magnitude in K_s (4) Logarithm of the total HI flux in Jy km s^{-1} based on Gavazzi et al. (2005) (5) Logarithm of the total gas mass in solar masses (6) Logarithm of the stellar mass in solar masses (7) Gas fraction (8) Oxygen abundance and uncertainty (9) Method of determining abundances: T_e -direct determination via $[\text{O III}]\lambda 4363$ (Osterbrock 1989); R_{23} -determination via the bright line method (McGaugh 1994) (10) Reference for abundances: V05: this work; VP03: Vilchez and Iglesias-Paramo (2003); KS97: Kobulnicky and Skillman (1997); M97: Martin (1997)

Table 6. Luminosity-metallicity relations for star-forming galaxies

Author (1)	Band (2)	Sample (3)	$L - Z$ Slope (4)	$L - Z$ Intercept (5)	rms (6)
SKH89	<i>B</i>	19 dIs	-0.153	5.500	0.16
RM95	<i>B</i>	12 dIs	-0.147 ± 0.029	5.670 ± 0.480	0.09
LMK03	<i>B</i>	22 dIs	-0.153 ± 0.025	5.590 ± 0.540	0.17
ZH06	<i>B</i>	21 dIs	-0.149 ± 0.011	5.650 ± 0.170	0.15
LMC04	<i>B</i>	$\times 100$ MP SFGs from 2dFGRS	-0.200 ± 0.020	4.290 ± 0.420	>0.3
LMC04	<i>B</i>	6387 SFGs from 2dFGRS	-0.223 ± 0.004	4.070 ± 0.090	0.32
THK04	<i>B</i>	~ 53000 SFGs from SDSS	-0.185 ± 0.001	5.238 ± 0.018	>0.3
SKL05	<i>B</i>	24 dwarf BCGs $M_B > -18$	-0.139 ± 0.011	5.800 ± 0.170	>0.2
SKL05	<i>B</i>	48 BCGs $M_B < -18$	-0.079 ± 0.018	6.930 ± 0.370	>0.2
SLM05	<i>B</i>	765 SFGs from KISS	-0.222 ± 0.003	4.180 ± 0.060	0.25
SLM05	<i>J</i>	420 SFGs from KISS	-0.200 ± 0.004	4.130 ± 0.090	0.22
SLM05	<i>K</i>	370 SFGs from KISS	-0.195 ± 0.004	4.030 ± 0.010	0.23
O06	<i>K</i>	29 dwarfs from Paper I and 2MASS	-0.140 ± 0.020	5.550 ± 0.260	0.15
V05	<i>J</i>	25 dIs	-0.140 ± 0.014	5.692 ± 0.214	0.11
V05	<i>K</i>	25 dIs	-0.141 ± 0.015	5.581 ± 0.244	0.10
V05	<i>J</i>	14 BCDs	-0.216 ± 0.027	4.530 ± 0.473	0.12
V05	<i>K</i>	14 BCDs	-0.224 ± 0.030	4.212 ± 0.537	0.11

Note. — (1) Reference: SKH89: Skillman, Kennicutt, & Hodge (1989); RM95: Richer and McCall (1995); LMK03: Lee et al. (2003a); ZH06: van Zee and Haynes (2006); LMC04: Lamareille et al. (2004); THK04: Tremonti et al. (2004); SKL05: Shi et al. (2005); SLM05: Salzer et al. (2005); O06: de Oliveira et al. (2006); V05: Vaduvescu 2005 (this work); (2) Observing Band (for the absolute magnitude); (3) Sample: SFGs: Star-Forming Galaxies; BCGs: Blue Compact Galaxies; MP: metal-poor ($12 + \log(\text{O}/\text{H}) \lesssim 8.3$); (4) $L - Z$ relation slope; (5) $L - Z$ relation intercept; (6) root mean square error in $\log(\text{O}/\text{H})$.

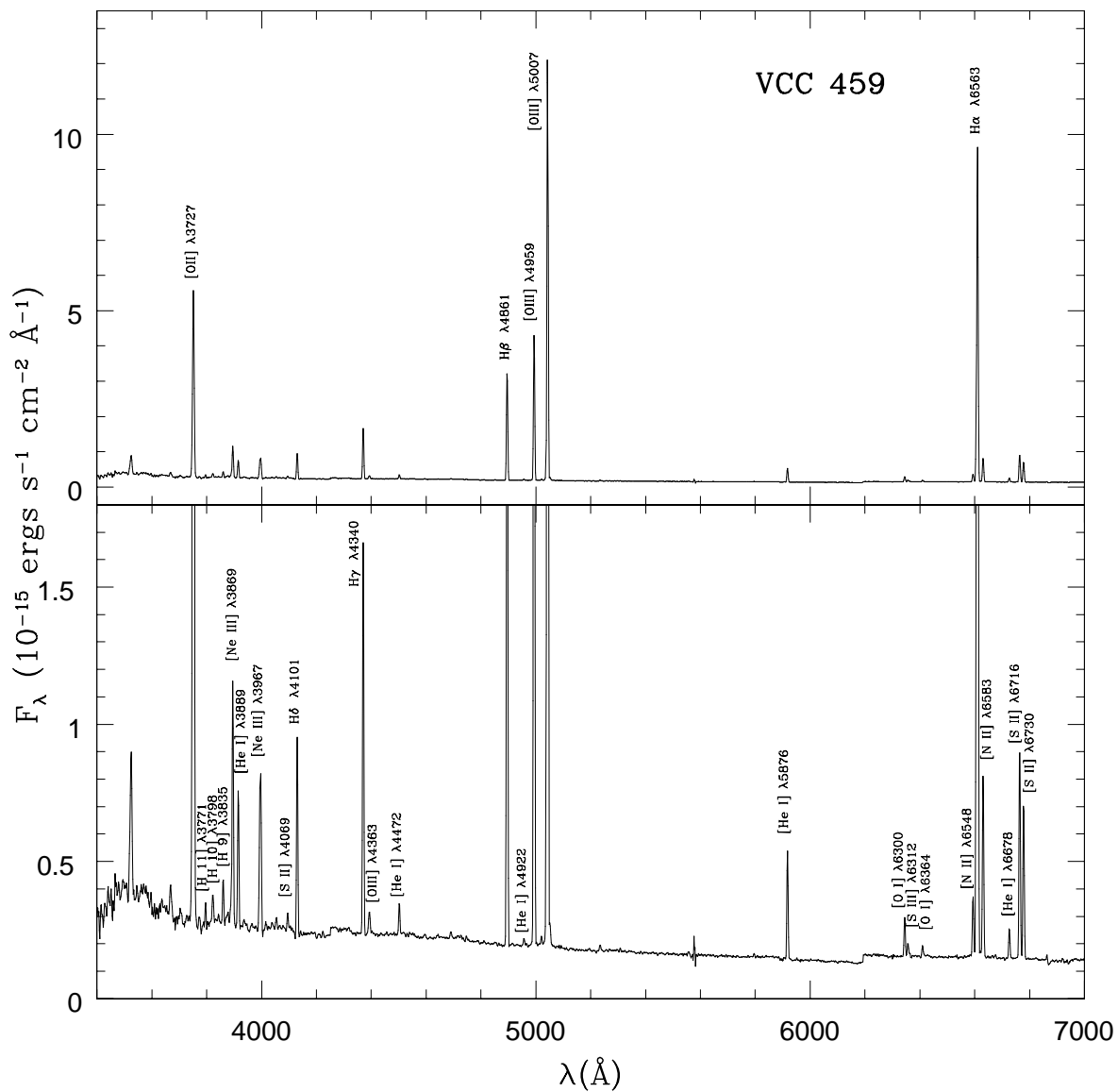


Fig. 1.— Reduced combined spectrum of VCC 459. For a better view of the lines, the spectra are shown at two vertical scalings. A “fracture” due to imperfect combination of the continua is visible at 6200 \AA . This did not affect measurements of the emission lines.

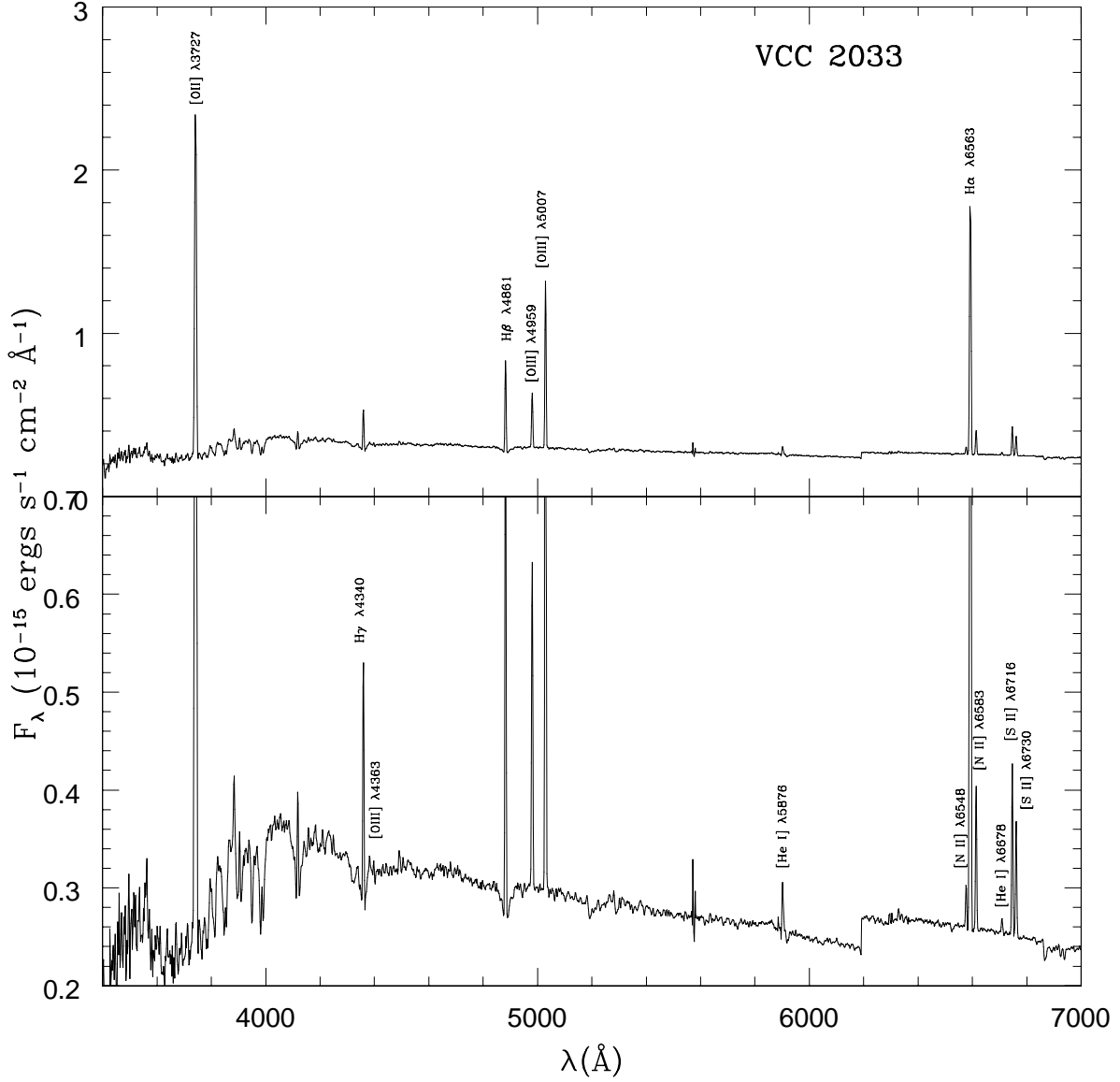


Fig. 2.— Reduced combined spectrum of VCC 2033. For a better view of the lines, the spectra are shown at two vertical scalings. A “fracture” due to imperfect combination of the continua is visible at 6200 \AA . This did not affect measurements of the emission lines.

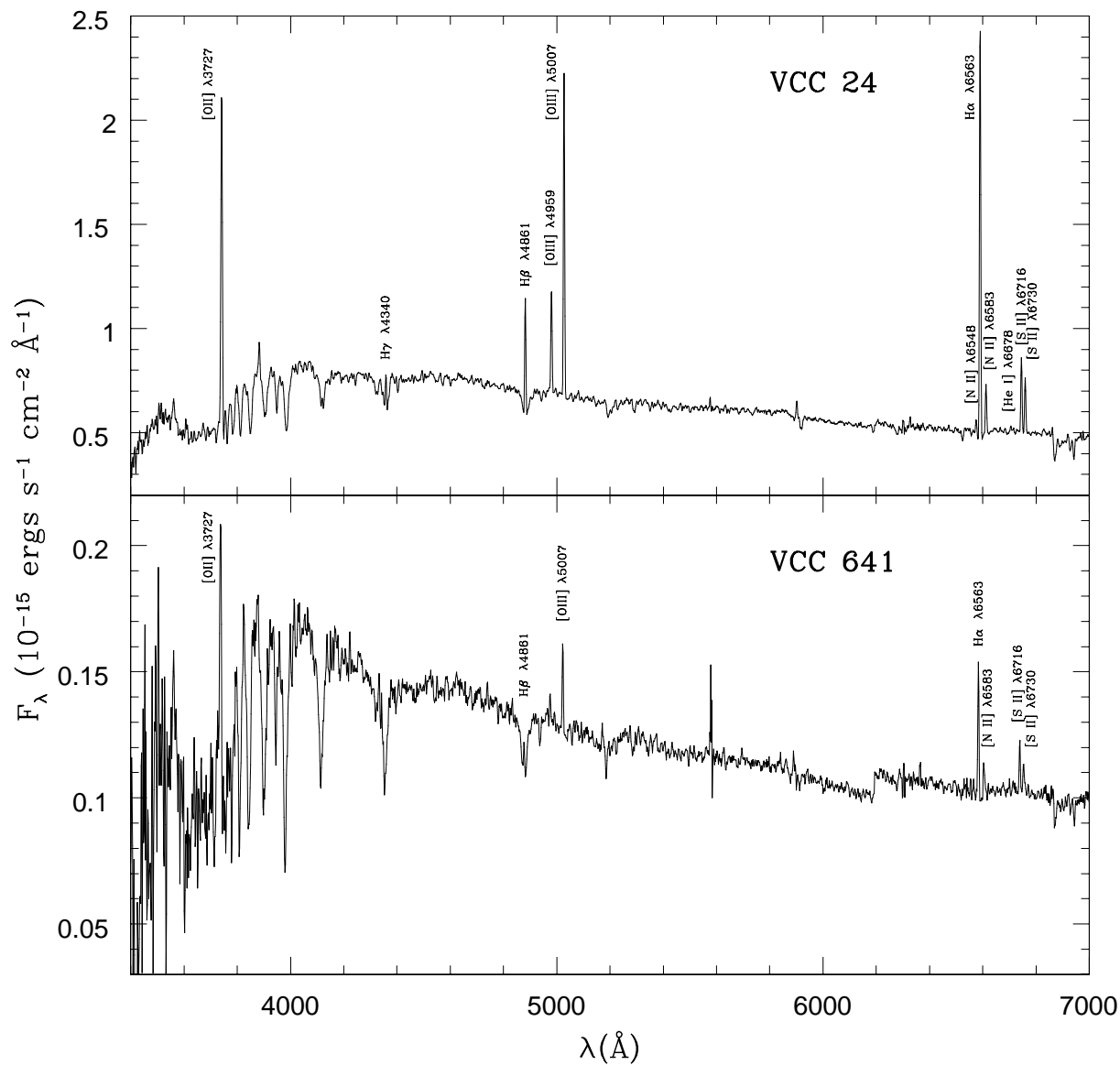


Fig. 3.— Reduced combined spectra of VCC 24 and VCC 641. A “fracture” due to imperfect combination of the continua of VCC 641 is visible at 6200 Å. This did not affect measurements of the emission lines.

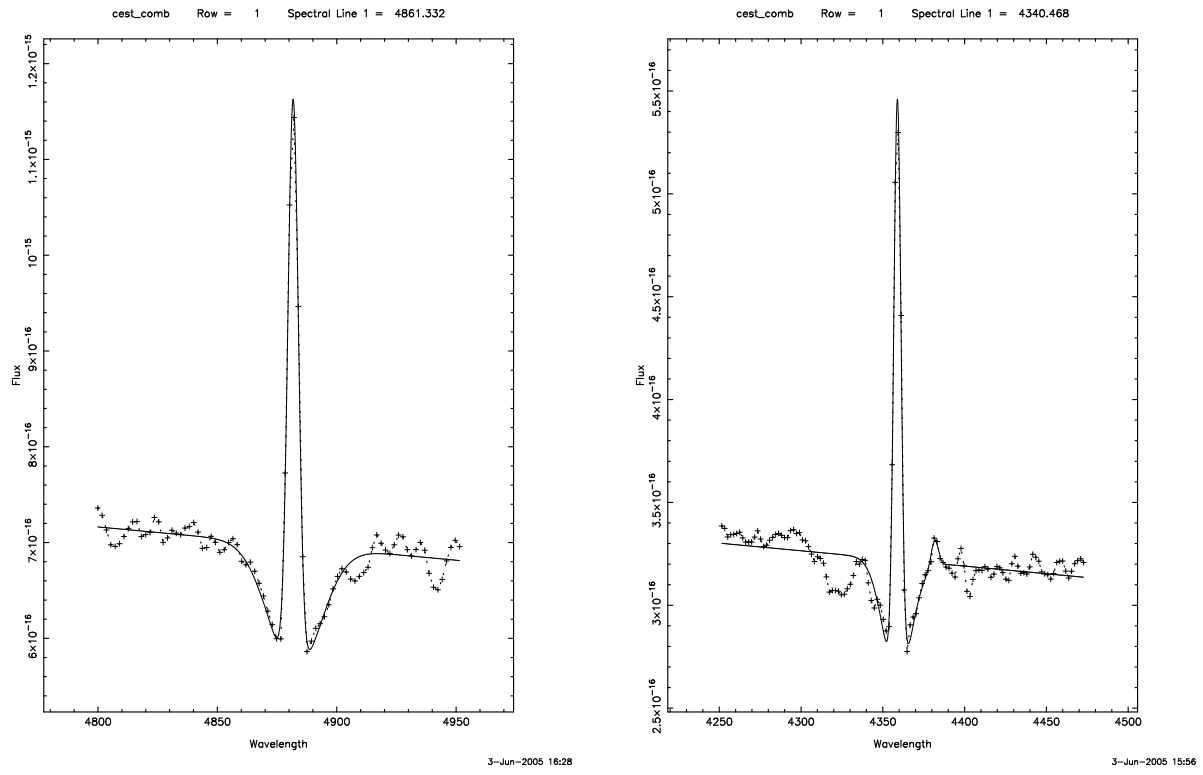


Fig. 4.— Flux versus wavelength for two INTENS fits. Left: $H\beta$ in VCC 24; Right: $H\gamma$ and $[OIII]\lambda 4363$ in VCC 2033. Pluses mark observations, and solid curves are fits.

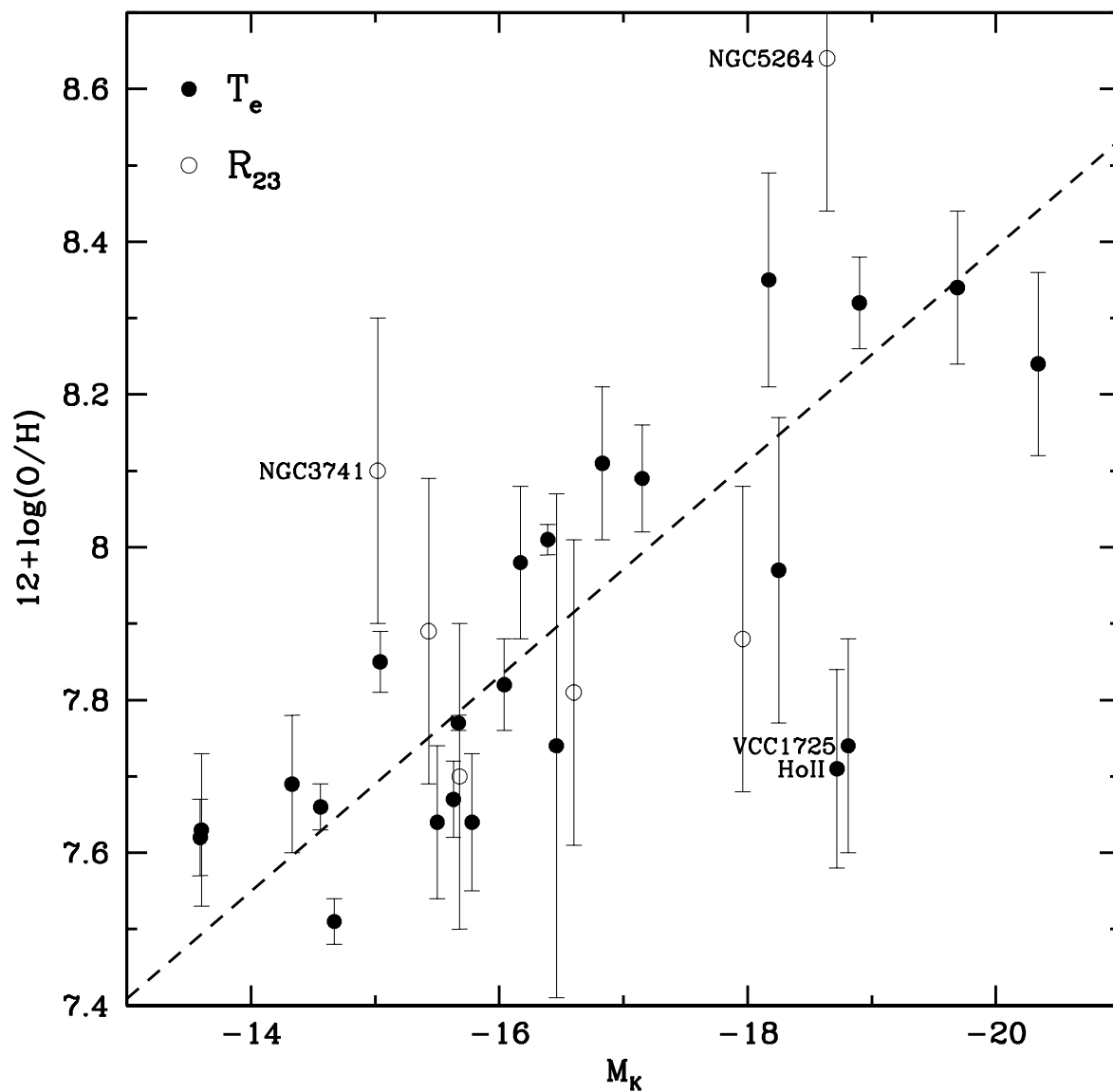


Fig. 5.— The oxygen abundance versus absolute sech magnitude in K_s for dIs. T_e -based abundances are plotted as solid symbols, and R_{23} -based abundances as open symbols. Errors in metallicities are shown as vertical bars. Typical errors for absolute magnitudes are ~ 0.1 mag. Four outliers are labeled in the plot. The geometric mean fit to other dIs is plotted as a dashed line.

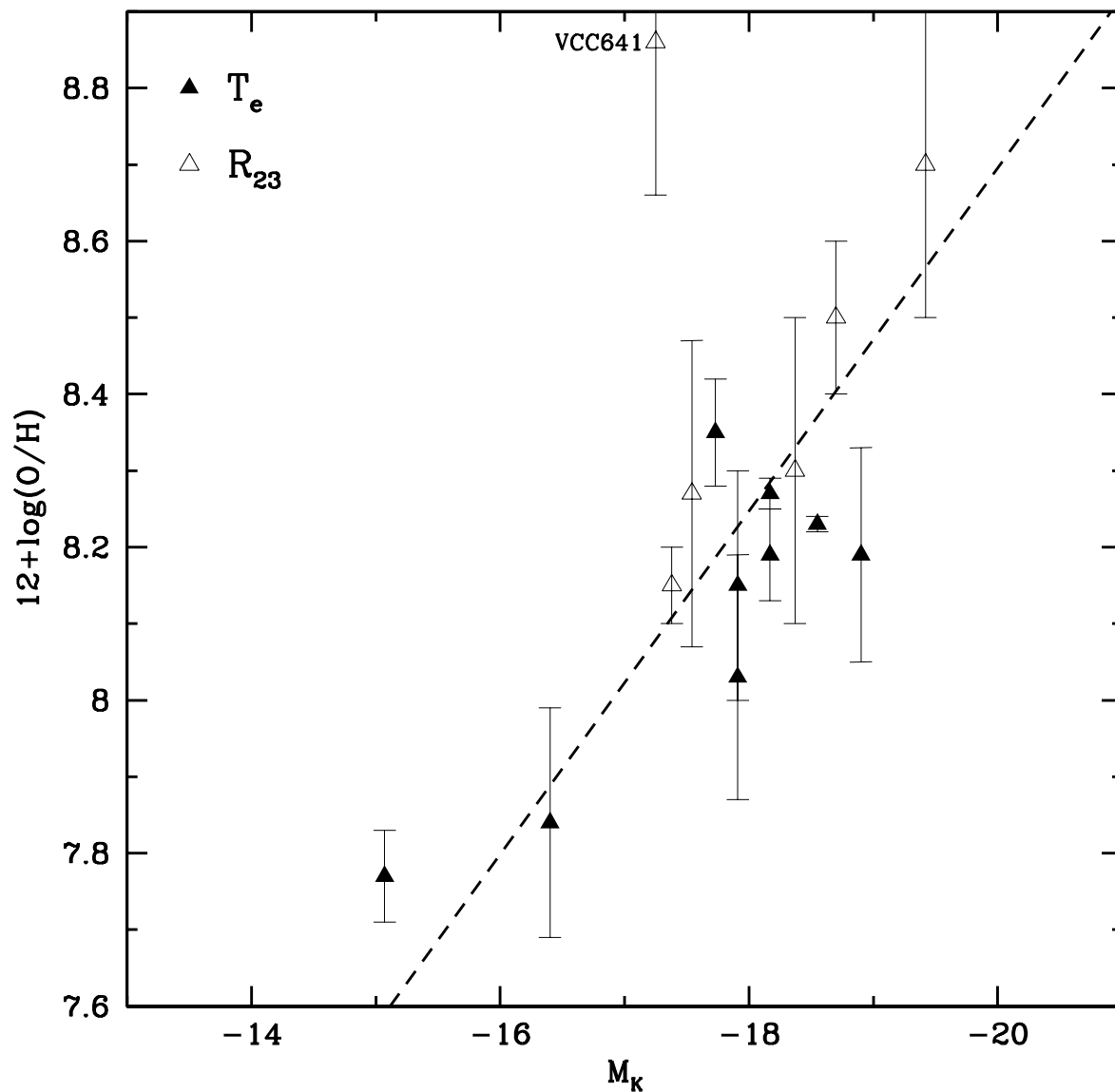


Fig. 6.— The oxygen abundance versus absolute sech magnitude in K_s for BCDs. T_e -based abundances are plotted as solid symbols, and R_{23} -based abundances as open symbols. We include errors in metallicities. Typical errors for absolute magnitudes are ~ 0.1 mag. One outlier is labeled. The geometric mean fit to the other BCDs is plotted as a dashed line.

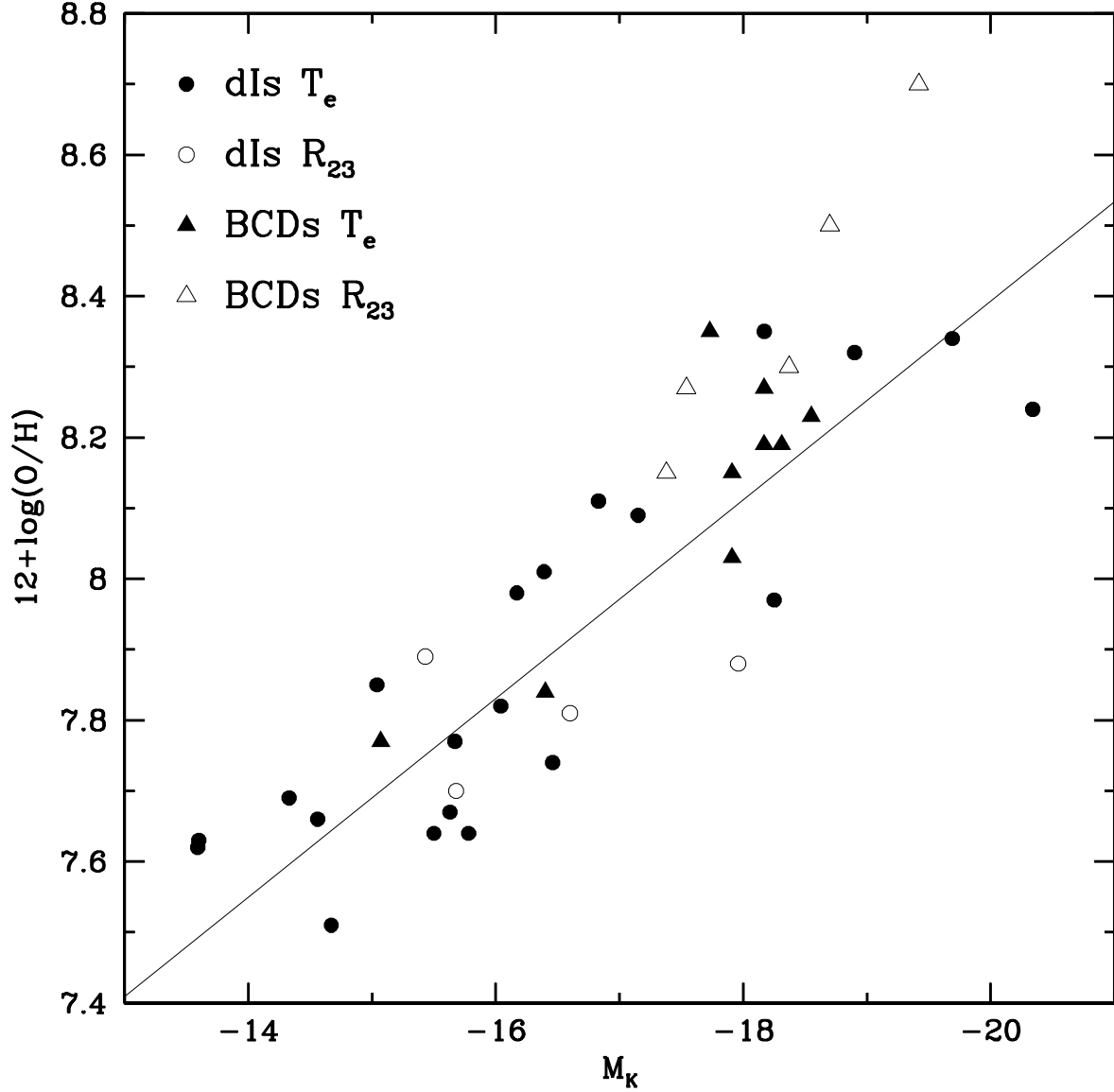


Fig. 7.— The oxygen abundance versus absolute sech magnitudes in K_s for dIs and BCDs. dIs are plotted as circles, while BCDs as triangles. T_e -based abundances are plotted as solid symbols, and R_{23} -based abundances as open symbols. The five outliers from Figures 5-6 are not shown. The solid line represents the $L - Z$ relation for the dIs.

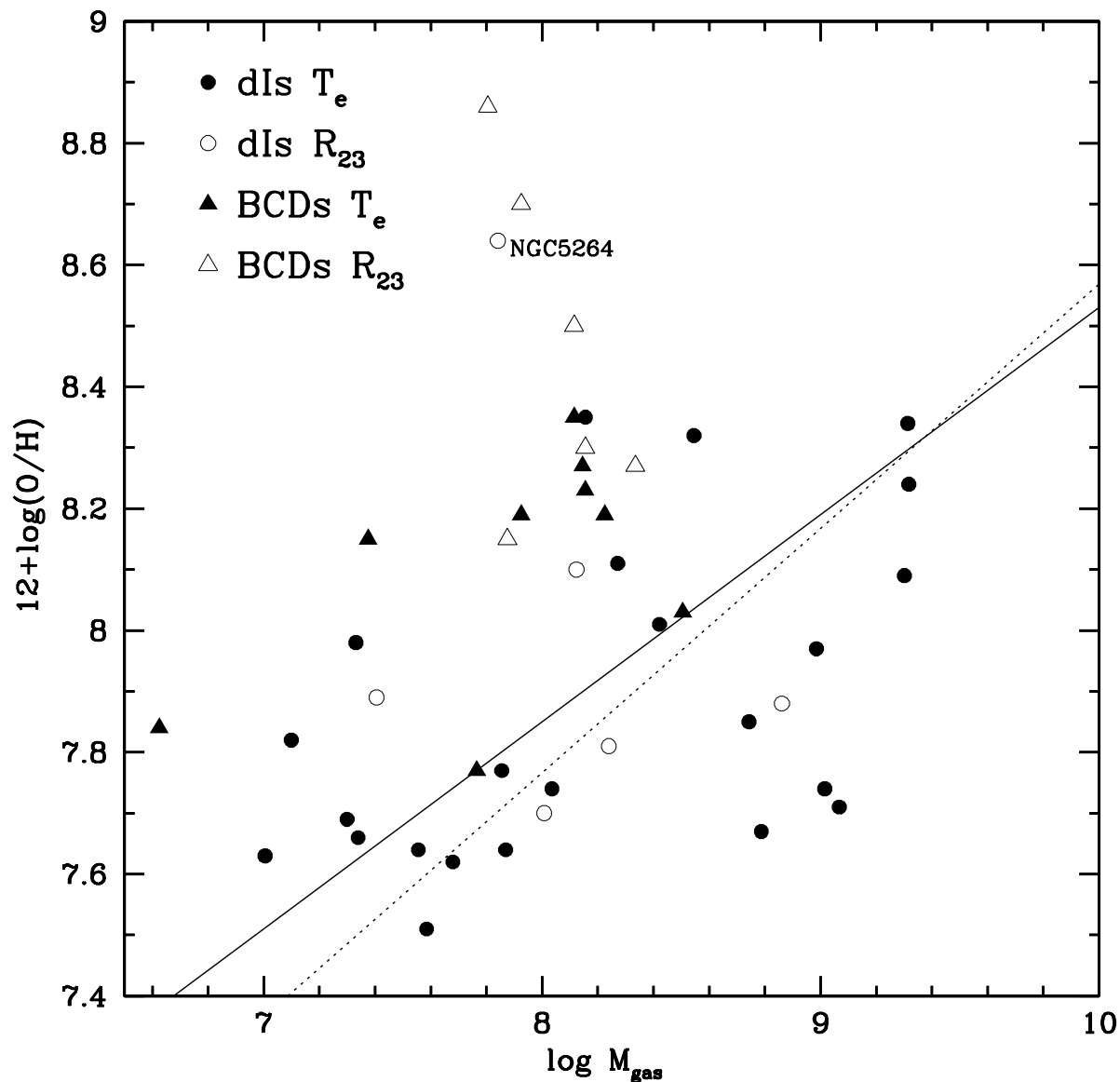


Fig. 8.— Correlation between oxygen abundance and the gas mass. dIIs are plotted with circles, and BCDs with triangles. T_e -based abundances are plotted as solid symbols, and R_{23} -based abundances as open symbols. dIIs with a greater gas mass are more abundant in metals. Ignoring NGC 5264, the geometric linear fit to the dII data is marked by a solid line. For comparison, the fit found by Lee et al. (2003a) is shown with a dotted line. BCDs often have less gas than dIIs at a given metallicity.

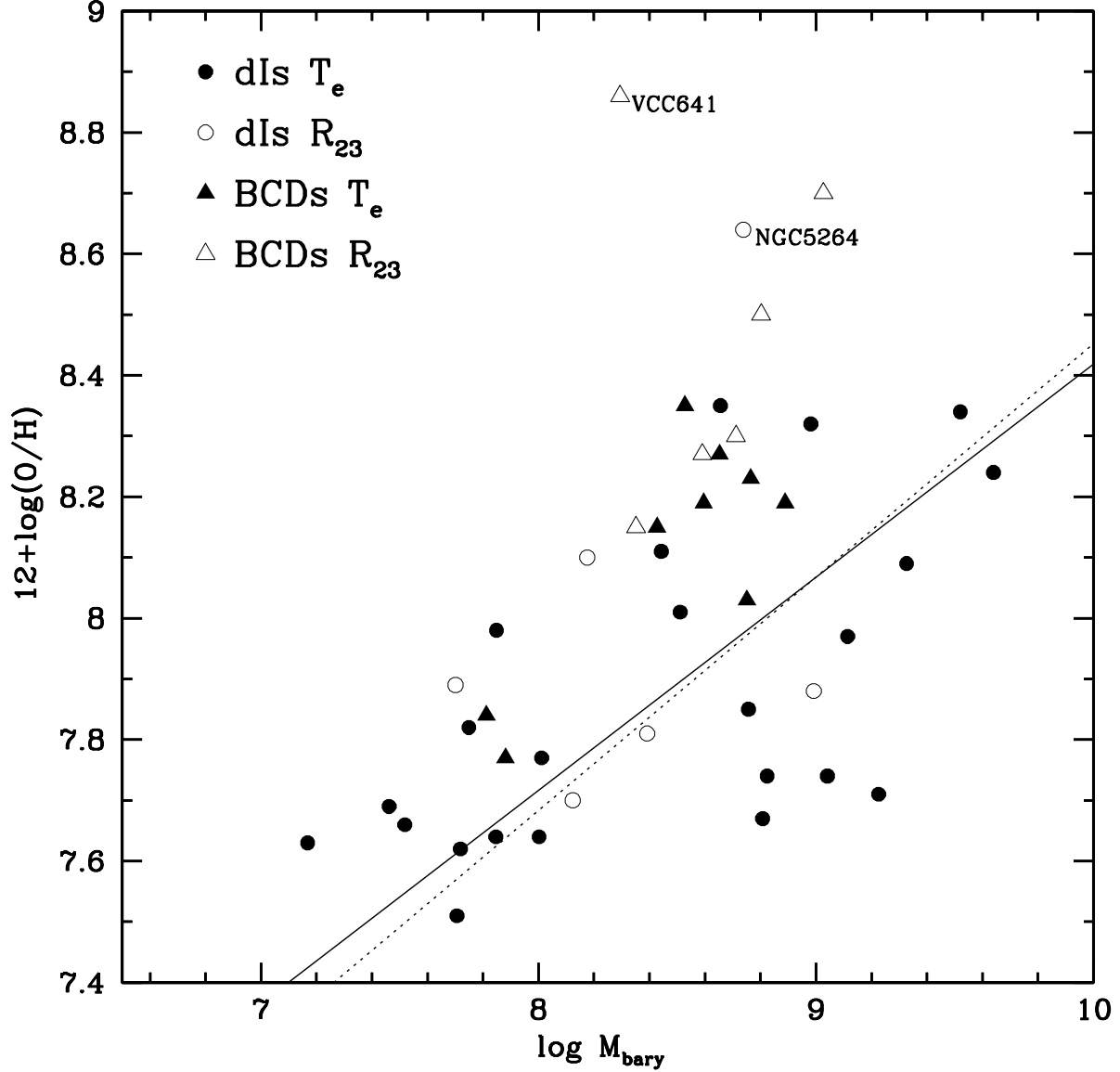


Fig. 9.— Correlation between oxygen abundance and baryonic mass. dIs are plotted with circles, and BCDs with triangles. T_e -based abundances are plotted as solid symbols, and R_{23} -based abundances as open symbols. Stellar masses were derived from sech magnitudes in K_s . More massive dIs are more abundant in metals. Ignoring NGC 5264, the geometric linear fit to the dI data is drawn as a solid line. For comparison, the Lee et al. (2003a) fit is plotted with a dashed line.

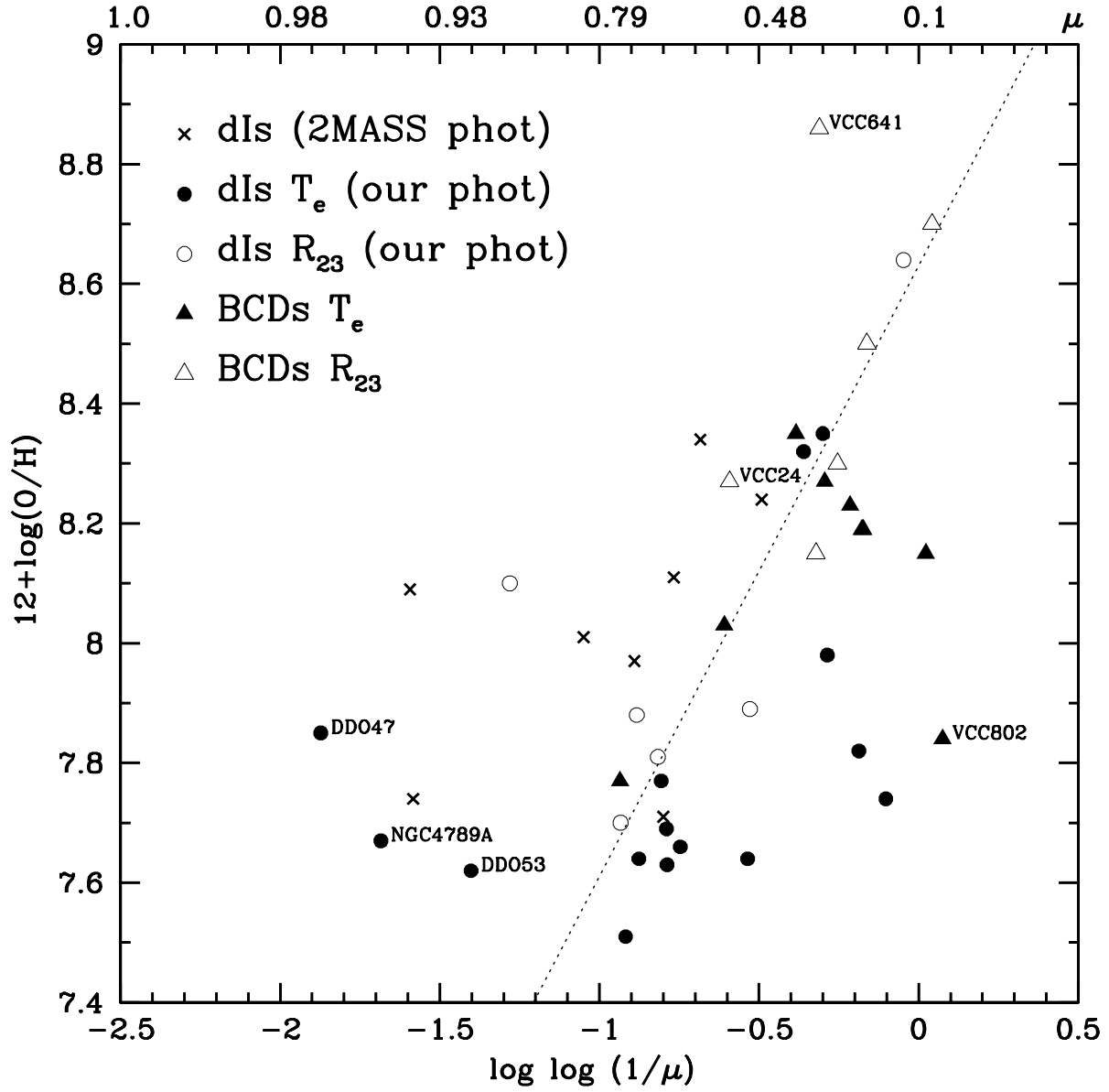


Fig. 10.— Correlation between oxygen abundance and the gas fraction, μ . dIs whose stellar masses were derived from sech magnitudes in K_s (Paper I) are plotted with circles, and while those derived from 2MASS photometry are plotted with crosses. BCDs, all of whose stellar masses were derived from sech magnitudes in K_s , are represented with triangles. T_e -based abundances are plotted as solid symbols and crosses, and R_{23} -based abundances as open symbols. The linear fit derived by Lee et al. (2003a) for his field dI sample is plotted with a dotted line. The gas fraction increases towards the left. Although there is a lot of scatter, most dIs and BCDs appear to follow the closed box model.